Transport properties of double-walled carbon nanotube quantum dots

Shidong Wang and Milena Grifoni
Theoretische Physik, Universität Regensburg, 93040 Regensburg, Germany
(Received 10 August 2007; revised manuscript received 20 December 2007; published 28 February 2008)

The transport properties of quantum dot (QD) systems based on double-walled carbon nanotubes (DWCNTs) are investigated. The interplay between microscopic structure and strong Coulomb interaction is treated within a bosonization framework. The linear and nonlinear current-voltage characteristics of the QD system are calculated by starting from the Liouville equation for the reduced density matrix. Depending on the intershell couplings, an eight-electron periodicity of the Coulomb blockade peak spacing in the case of commensurate DWCNT QDs and a four-electron periodicity in the incommensurate case are predicted. The contribution of excited states of DWCNTs to the nonlinear transport is investigated as well.

DOI: 10.1103/PhysRevB.77.085431 PACS number(s): 73.63.Fg, 73.23.Hk, 71.10.Pm

I. INTRODUCTION

After being discovered in 1991,[1] carbon nanotubes (CNTs) have been widely used in nanodevices because of their unique properties.[2–4] CNTs may be either single walled (SWCNT) or multiwalled (MWCNT) depending on the number of graphene sheets wrapped into concentric cylinders. Due to the quasi-one-dimensional characters of their electronic structures, long SWCNTs exhibit a Luttinger-liquid behavior.[5–12] SWCNT quantum dot (QD) systems have also been fabricated, which consist of finite length SWCNTs weakly connected to the source and drain leads and capacitively coupled to a gate electrode.[13–16] At low bias, SWCNT QD systems show Coulomb blockade because of the strong Coulomb interactions in the QDs and the poor transparencies of the contacts between the QD and the leads.[17] Because of the short lengths of SWCNTs, the addition energy needed to add an extra electron to the QD depends on both the Coulomb interaction and on the energy level spacing. Unlike the traditional two-dimensional semiconductor QD systems with irregular Coulomb blockade patterns, which have to be understood statistically,[18] QDs based on SWCNTs show regular Coulomb blockade patterns, which originate from the regular electronic structure of the SWCNTs. Because of the spin degeneracy of two bands crossing at the Fermi points in metallic SWCNTs, the stability diagrams of SWCNT QDs exhibit a four-electron periodicity of the Coulomb diamond sizes.[13–16,19] The stability diagrams of the SWCNT QD systems have been explained by using the mean-field theory developed in Ref. 20 which includes a nonzero exchange energy.[13–16] Recently, the energy spectrum of SWCNT QDs has been calculated in Ref. 21 beyond mean field. For QD systems with moderate-to-large radius SWCNTs, the exchange energy can be ignored[21] and the stability diagrams can also be quantitatively explained within a bosonization approach.[22,23] By suitable choice of parameters, these theories can reproduce the *same* low bias spectra of SWCNT QDs, and only the excitations measured at high bias are predicted differently by a mean-field approach or by a bosonization method because of the different treatment of the Coulomb interaction.[23] Although the excitations of SWCNT QDs have already been measured,[15] the quality and the range of the measured excitations cannot be used to determine the validity of these two methods and further experiments are needed.

In contrast, the properties of MWCNT systems have not been fully explored so far. Experimental evidences of strong Coulomb interactions, manifesting themselves in zero-bias anomalies, power-law behaviors, and Coulomb blockade, have been reported.[24–28] In particular, the experiment in Ref. 28 showed that the stability diagrams of MWCNT QDs with many shells systems have a four-electron periodicity of the Coulomb diamond sizes. A microscopic description of interacting MWCNT has been provided so far for ideally infinite systems only.[29–31] The simplest MWCNT is the one formed by a double-walled carbon nanotube (DWCNT), which consists of two concentric shells. Depending on the ratio between the unit cell lengths of the two shells, a DWCNT may be either commensurate (c-DWCNT), if the ratio is a commensurate number, or incommensurate (i-DWCNT), if the ratio is an incommensurate number. It has been shown that the effective intershell coupling depends on the type of DWCNTs. At low energies, that is, near the Fermi energy, the effective intershell coupling is negligible in i-DWCNTs but large in c-DWCNTs while it cannot be ignored in both types of DWCNTs at high energies.[31–34] Both types of DWCNTs with long lengths can be described by the Luttinger-liquid theory when Coulomb interactions are included.[31]

As mentioned above, a theory for interacting finite size DWCNTs has not been provided so far and is the subject of the present work. Because of their intermediate-to-large radii, we expect that the exchange energy may be neglected in DWCNTs. Therefore, the bosonization approach, which includes forward-scattering processes exactly, can be used to describe the properties of DWCNT QD systems as well. In this paper, we focus on a QD system formed by a finite length DWCNT with two metallic shells, where we include all forward-scattering processes. The bosonization approach enables exact diagonalization of the interacting DWCNT Hamiltonian. Finally, the linear and nonlinear transport properties of the system are investigated by solving the Liouville equation for the reduced density matrix to lowest order in the coupling to the leads.

The paper is organized as follows. In Sec. II, the Hamiltonian of a DWCNT QD system is derived. The energy spectrum of a finite length DWCNT with strong Coulomb interactions and open boundary conditions is then obtained.

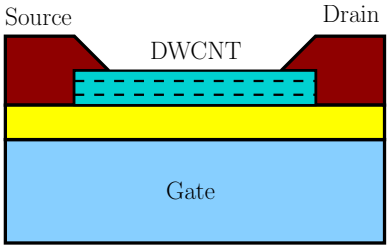

FIG. 1. (Color online) Schematic experimental setup of a DWCNT QD system. A finite length DWCNT is deposited on a substrate and weakly connected to the source and drain leads through its outer shell. A gate electrode is capacitively coupled to the DWCNT QD and controls the electrochemical potential in the QD. The dashed lines denote the inner shell in the DWCNT.

Transport properties of DWCNT QDs are calculated in Sec. III. The results for the linear and nonlinear conductances of both c-DWCNT and i-DWCNT QDs are presented in Sec. IV. Finally, the conclusion is drawn in Sec. V.

II. MODEL AND METHOD

As schematically shown in Fig. 1, the QD system consists of a DWCNT with two metallic shells deposited on a substrate. The source and drain leads are connected to the outer shell of the DWCNT. The segment of the DWCNT between two leads forms a QD. A gate electrode is capacitively coupled to the QD and controls the electrochemical potential in it. As we are only interested in the Coulomb blockade regime, we assume that the QD is weakly contacted to two leads, that is, the transparencies of the contacts are very poor and the conductance of the QD system is much smaller than the conductance quantum $2e^2/h$. The Hamiltonian of the whole system can be separated into several parts,

$$H = H_{\text{leads}} + H_{\text{DWCNT}} + H_T + H_g, \tag{1}$$

where H_{DWCNT} is the Hamiltonian of the DWCNT system and its explicit form will be derived in the following subsection. The source (s) and drain (d) leads are described by Fermi gases of noninteracting quasiparticles and the Hamiltonian of the leads is

$$H_{\text{leads}} = \sum_{l=s,d} \sum_{\mathbf{k}\sigma} (\varepsilon_{l\mathbf{k}} - eV_l) c^\dagger_{l\mathbf{k}\sigma} c_{l\mathbf{k}\sigma}, \tag{2}$$

where e is the elementary charge and V_l is the voltage in the lead l. The operators $c^\dagger_{l\mathbf{k}\sigma}$ and $c_{l\mathbf{k}\sigma}$ are the creation and annihilation operators of a quasiparticle with wave vector $\mathbf{k}$ and spin $\sigma = \pm$ in the lead l. The Hamiltonian of the gate is

$$H_g = -e\mu_g \mathcal{N},$$

where μ_g is the chemical potential of the gate and the operator $\mathcal{N}$ accounts for the total electron number in the QD system. H_T is the tunneling Hamiltonian describing the tunneling between the DWCNT and the two leads and it has the form

$$H_T = \sum_{l=s,d} \sum_{\beta\sigma} \int d\mathbf{r} T_{l\beta}(\mathbf{r}) \Psi^\dagger_{\beta\sigma}(\mathbf{r}) \Phi_{l\sigma}(\mathbf{r}) + \text{H.c.}, \tag{3}$$

where $\Phi_{l\sigma}(\mathbf{r}) = \Sigma_{\mathbf{k}} \phi_{\mathbf{k}}(\mathbf{r}) c_{\mathbf{k}l\sigma}$ is the electron annihilation operator in the lead l and $\Psi^\dagger_{\beta\sigma}(\mathbf{r})$ is the electron operator in the shell β whose explicit form will be given in Sec. II B. In the remaining of this section, we are going to discuss the specific form of H_{DWCNT}. Specifically, we are going to first express it as the sum of a noninteracting and an interacting part, $H_{\text{DWCNT}} = H^0_{\text{DWCNT}} + H^{\text{int}}_{\text{DWCNT}}$, and then we shall diagonalize it by using a bosonization procedure.

A. Low energy noninteracting Hamiltonian of double-walled carbon nanotubes

In general, the energy spectrum of a SWCNT or of a DWCNT without electron-electron interactions can be obtained by using a tight-binding model for the p_z orbitals in carbon atoms.[2] In particular, we shall view in the following a DWCNT as two tunneling coupled SWCNT shells. We denote with the index $\beta = \pm$ the outer (inner) SWCNT shell.

Let us then start, following Ref. 23, to recall the Bloch wave functions describing a SWCNT in shell β in the case of periodic boundary condition (PBC) and open boundary condition (OBC). The latter case is the proper choice for the description of finite size SWCNTs and DWCNTs.

SWCNT with periodic boundary conditions. The spectrum of a metallic SWCNT shell β within periodic boundary conditions has two independent Fermi points ($\pm K_{0,\beta}$). Their positions depend on the chirality of the shell and in general are different for different SWCNT shells. At the Fermi points, the lowest conduction and the highest valence bands touch each other, as shown in Fig. 2(a). As the next conduction and valence bands are separated by a large gap (about 1 eV),[2] we will only consider the lowest conduction band and the highest valence band in our calculations. The energy dispersion near the Fermi points is linear,[2] see Fig. 2(a), and is given by

$$\varepsilon_{R/L}(\kappa) = \pm \hbar v_F \kappa, \tag{4}$$

where the wave vector κ is measured with respect to the Fermi points and the Fermi velocity in SWCNTs is $v_F \approx 8 \times 10^5$ m/s. Hence, at each Fermi point, there are two branches corresponding to right and left moving electrons characterized by the index $r = R/L = \pm$. The Bloch waves for the electrons in these branches in a shell $\beta = \pm$ are

$$\varphi_{\beta r F \kappa}(\mathbf{r}) = e^{i\kappa u} \varphi_{\beta r F}(\mathbf{r}), \tag{5}$$

where $\mathbf{r} = (u, v)$ and u and v are along the nanotube axis and the circumference directions, respectively (cf. Fig. 3). The periodic part of the Bloch wave is constructed from the p_z orbital wave function $\chi(\mathbf{r})$ as

$$\varphi_{\beta r F}(\mathbf{r}) = \frac{1}{\sqrt{N_\beta}} \sum_{\mathbf{R}p} e^{i\mathbf{F}\cdot\mathbf{R}} f_{\beta p r F} \chi(\mathbf{r} - \mathbf{R} - \tau_p), \tag{6}$$

where the index $\mathbf{R}$ denotes the lattice vector of the graphene sheet, N_β is the number of carbon atoms in the shell β, $p = \pm$ is the index for the two graphene sublattices, and $\boldsymbol{\tau}_p$ is the vector giving the positions of the two different atoms in a

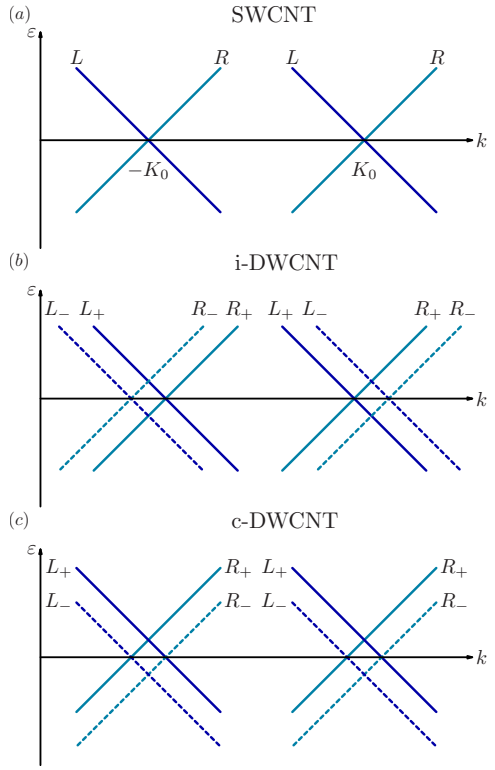

FIG. 2. (Color online) Energy spectra of metallic SWCNT and DWCNT with PBCs. (a) Energy spectrum of a metallic SWCNT. There are two Fermi points and two branches L/R with left-moving (right-moving) electrons at each Fermi point. (b) Energy spectrum of an i-DWCNT. It consists of the energy spectra of the outer and inner graphene shells ($\pm$), which are not coupled to each other because of the vanishing intershell coupling, cf. Eq. (12). (c) Energy spectrum of a c-DWCNT. Because of the finite intershell coupling, it is composed of the bonding and antibonding bands ($\pm$), which are shifted vertically along the ε axis, cf. Eq. (15).

unit cell. The index $F=\pm K_{0,\beta}$ characterizes the Fermi points in the spectrum of the shell β and $\mathbf{F}$ denotes the Fermi points in a graphene sheet. They are related by $F \equiv \mathbf{F}\cdot\mathbf{u}$ with $\mathbf{u}$ the unit vector along the nanotube axis. Finally, the coefficients f depend on the chirality of the shell (m,n) and read[2]

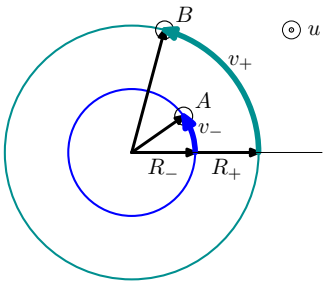

FIG. 3. (Color online) Cross section of a DWCNT. Atoms A and B in two shells of radii R_+ and R_-, respectively, are projected onto this cross section. Such atoms are described by the coordinates (u_+,v_+) and (u_-,v_-), where $u_\pm$ are along the tube axis and $v_\pm$ measure the atom positions on the outer (inner) circumference.

$$f_{\beta+rF} = \frac{1}{\sqrt{2}\mathcal{L}}\left[-\frac{\sqrt{3}}{2}\,\mathrm{sgn}(Fr)(n+m) + \frac{i}{2}\,\mathrm{sgn}(r)(m-n)\right], \tag{7}$$

$$f_{\beta-rF} = \frac{1}{\sqrt{2}}, \tag{8}$$

where $\mathcal{L}=\sqrt{n^2+mn+m^2}$.

SWCNT with open boundary conditions. Because we consider a finite length shell, we have to use the OBC instead of the periodic boundary condition along the tube axis (cf. Fig. 4). The standing wave in the shell β satisfying the OBC is obtained by a suitable combination of PBC wave functions[23]

$$\varphi^{\mathrm{OBC}}_{\beta\tilde{R}/\tilde{L}\kappa}(\mathbf{r}) := \frac{1}{\sqrt{2}}[\varphi_{\beta R/LK_0\kappa}(\mathbf{r}) - \varphi_{\beta L/R-K_0-\kappa}(\mathbf{r})], \tag{9}$$

and the wave vectors κ are quantized as

$$\kappa = \frac{\pi}{L}(m_\kappa + \Delta_\beta), \quad m_\kappa = 0, \pm 1, \pm 2, \ldots, \tag{10}$$

where L is the length of the nanotube. For each shell, we introduce the offset parameter Δ_β which characterizes the mismatch of the Fermi points, $0 \leqslant \Delta_\beta = K_{0,\beta}L/\pi - [K_{0,\beta}L/\pi] < 1$, where $[\cdots]$ gives the integer part of its argument. As shown in Fig. 4, it is responsible for a possible mismatch of the energy levels between the $\tilde{R}$ and $\tilde{L}$ branches defined by the relation Eq. (9). The Hamiltonian of a finite length noninteracting shell β is thus

$$H^0_\beta = \sum_{\tilde{r}\sigma\kappa} \mathrm{sgn}(\tilde{r})\hbar v_F \kappa c^\dagger_{\beta\tilde{r}\kappa\sigma} c_{\beta\tilde{r}\kappa\sigma}, \tag{11}$$

where $\tilde{r}=\tilde{R}/\tilde{L}=\pm$ is the index for the left and right moving electrons with the OBC. The operators $c^\dagger_{\beta\tilde{r}\kappa\sigma}$ and $c_{\beta\tilde{r}\kappa\sigma}$ are the creation and annihilation operators of an electron in the shell β, on branch $\tilde{r}$, with the wave vector κ and spin $\sigma = \uparrow, \downarrow$.

DWCNT with open boundary conditions. Let us now see how the spectrum gets modified when looking at DWCNTs, being two coaxial SWCNT shells. Neglecting for the moment Coulomb interactions, coupling between the two shells can occur due to intershell tunneling. It has been shown in previous works that the intershell coupling strongly depends on the chirality of the two shells.[31–33,35–37] Specifically, two shells are called incommensurate (commensurate) if the ratio between their respective unit cells along the tube axis is irrational (rational). In particular, helicity dependent selection rules prevent, at low energies, intershell tunneling in a DWCNT with incommensurate shells (i-DWCNT).[31] In contrast, intershell tunneling is always possible in c-DWCNTs.

Therefore, the noninteracting Hamiltonian of an i-DWCNT is the sum of the Hamiltonians of the two shells, while for c-DWCNTs, the intershell coupling must be included which yields a modification of the spectrum of the isolated SWCNT shells. The DWCNT spectra with PBC and

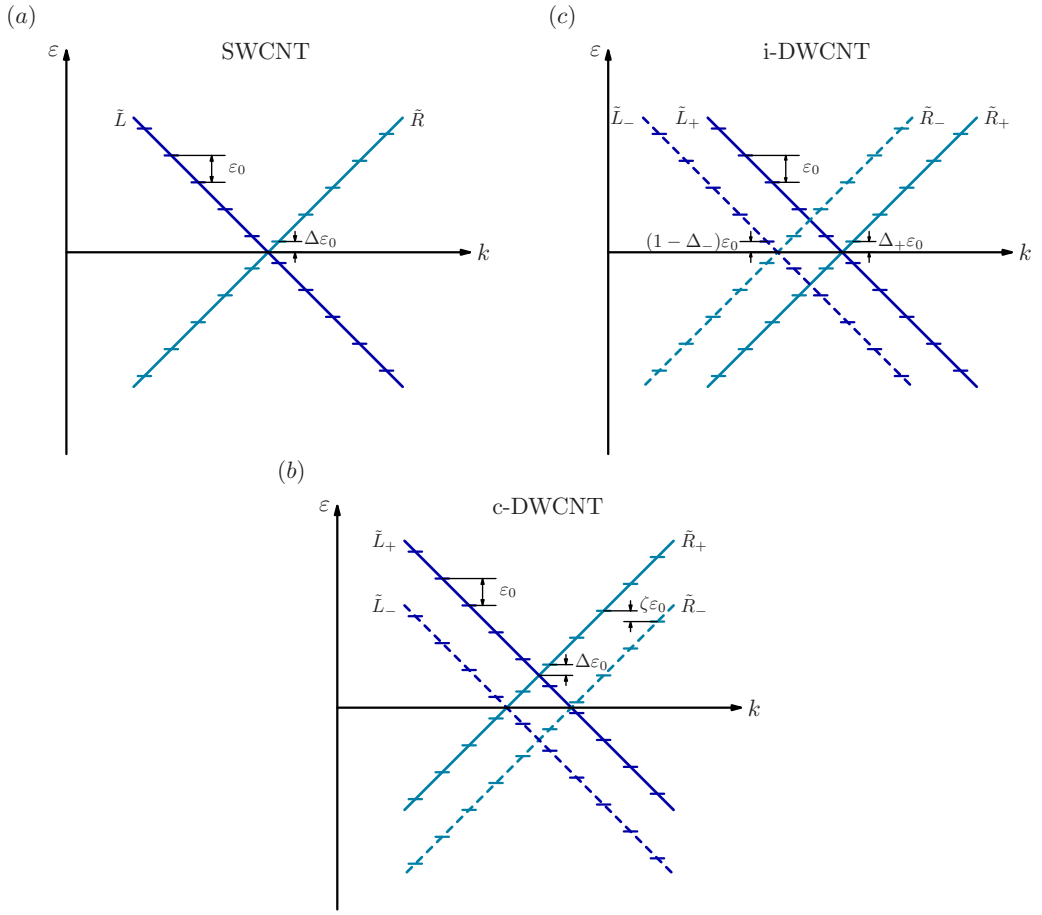

FIG. 4. (Color online) Energy spectra of metallic SWCNT and DWCNT with OBCs. (a) Energy spectrum of a metallic SWCNT. There are two branches $\tilde{L}/\tilde{R}$ with left (right) moving electrons. The parameter ε_0 is the level spacing and Δ describes the mismatch of the Fermi point, cf. Eq. (10). (b) Energy spectrum of an i-DWCNT and (c) of a c-DWCNT. The parameter $\Delta_\pm$ describes the mismatch of the Fermi point in the shell $\pm$ and for a c-DWCNT is $\Delta_+=\Delta_-=\Delta$. The parameter ζ describes the mismatch of the states in two bands, cf. Eq. (16).

OBC are depicted in Figs. 2(b), 2(c), 4(b), and 4(c), respectively. In particular, the i-DWCNT Hamiltonian associated with the OBC spectrum is

$$H^0_{\text{i-DWCNT}} = \sum_{\beta\tilde{r}\sigma\kappa} \text{sgn}(\tilde{r})\hbar v_F \kappa c^\dagger_{\beta\tilde{r}\kappa\sigma} c_{\beta\tilde{r}\kappa\sigma} = \sum_{\beta\tilde{r}\sigma m_\kappa} \text{sgn}(\tilde{r})(m_\kappa\varepsilon_0 + \Delta_\beta\varepsilon_0) c^\dagger_{\beta\tilde{r}\kappa\sigma} c_{\beta\tilde{r}\kappa\sigma}, \quad (12)$$

where $\varepsilon_0=\hbar v_F\pi/L$ is the level spacing and we have used the quantization relation for κ, Eq. (10) [cf. Fig. 4(b)]. The noninteracting Hamiltonian of a c-DWCNT contains also the contribution from the intershell coupling[31] and reads

$$H^0_{\text{c-DWCNT}} = \sum_\beta \sum_{\tilde{r}\sigma\kappa} \text{sgn}(\tilde{r})\hbar v_F \kappa c^\dagger_{\beta\tilde{r}\kappa\sigma} c_{\beta\tilde{r}\kappa\sigma} + \sum_{\beta\beta'} \sum_{\tilde{r}\sigma\kappa} t c^\dagger_{\beta\tilde{r}\kappa\sigma} c_{\beta'\tilde{r}\kappa\sigma} + \text{H.c.}, \quad (13)$$

where t is the intershell coupling and we assume that it is a constant in the low energy regime. The Hamiltonian [Eq. (13)] can be diagonalized by using the bonding and antibonding basis,

$$\tilde{c}_{\nu\tilde{r}\kappa\sigma} = \frac{1}{\sqrt{2}}[c_{+\tilde{r}\kappa\sigma} + \text{sgn}(\nu) c_{-\tilde{r}\kappa\sigma}],$$

$$\tilde{c}^\dagger_{\nu\tilde{r}\kappa\sigma} = \frac{1}{\sqrt{2}}[c^\dagger_{+\tilde{r}\kappa\sigma} + \text{sgn}(\nu) c^\dagger_{-\tilde{r}\kappa\sigma}], \quad (14)$$

where $\nu=\pm$ is the index for bonding and antibonding states, respectively. The noninteracting Hamiltonian of a c-DWCNT in the new basis becomes

$$H^0_{\text{c-DWCNT}} = \sum_{\nu\tilde{r}\sigma\kappa} [\text{sgn}(\tilde{r})\hbar v_F\kappa + \text{sgn}(\nu)t]\tilde{c}^\dagger_{\tilde{r}\nu\kappa\sigma}\tilde{c}_{\tilde{r}\nu\kappa\sigma} = \sum_{\nu\tilde{r}\sigma m_\kappa} [\text{sgn}(\tilde{r})(m_\kappa\varepsilon_0 + \Delta\varepsilon_0) + \text{sgn}(\nu)\zeta\varepsilon_0]\tilde{c}^\dagger_{\tilde{r}\nu\kappa\sigma}\tilde{c}_{\tilde{r}\nu\kappa\sigma}, \quad (15)$$

where for c-DWCNT is $\Delta_\beta=\Delta$ and the parameter ζ is defined as

$$0 \leqslant \zeta = t/\varepsilon_0 - [t/\varepsilon_0] < 1, \quad (16)$$

which describes the mismatch of states in two bands [cf. Fig. 4(c)].

B. Coulomb interaction Hamiltonian of double-walled carbon nanotubes

In quasi-one-dimensional electronic structures as CNTs, Coulomb interactions are not fully screened and can strongly influence the properties of CNTs, as amply demonstrated for SWCNTs.[5–9,13–16,22,23] On multiwalled nanotubes, despite the experimental evidence of strong Coulomb interactions,[24–28] not much is known theoretically.[29–31] In a previous work, we discussed the Luttinger-liquid nature of ideally infinite DWCNT;[31] here, we focus on the properties of finite size interacting DWCNT systems.

Let us start by looking at i-DWCNTs. Since in this case the two shells are not coupled by intershell tunneling, we can express the total Coulomb interaction by the Hamiltonian

$$H^{\text{int}}_{\text{i-DWCNT}} = \frac{1}{2}\sum_{\beta\beta'\sigma\sigma'}\int\int d\mathbf{r}_1 d\mathbf{r}_2 \Psi^{\dagger}_{\beta\sigma}(\mathbf{r}_1)\Psi^{\dagger}_{\beta'\sigma'}(\mathbf{r}_2) \times U_{\beta\beta'}(\mathbf{r}_1-\mathbf{r}_2)\Psi_{\beta'\sigma'}(\mathbf{r}_2)\Psi_{\beta\sigma}(\mathbf{r}_1), \tag{17}$$

where the electron operator for the shell β is

$$\Psi_{\beta\sigma}(\mathbf{r}) \equiv \sum_{\tilde{r}q}\varphi^{\text{OBC}}_{\beta\tilde{r}q}(\mathbf{r})c_{\beta\tilde{r}\sigma q}. \tag{18}$$

Here, $\mathbf{r}_i=(u_i,v_i)$ and u and v are along the tube axis and the circumference direction, respectively (cf. Fig. 3). The *intrashell* interaction is given by

$$U_{\beta\beta}(\mathbf{r}_1-\mathbf{r}_2) = \frac{e^2/\epsilon}{\sqrt{(u_1-u_2)^2+4R_\beta^2\sin^2[(v_1-v_2)/2R_\beta]+a_z^2}}, \tag{19}$$

and the *intershell* interaction is

$$U_{+-}(\mathbf{r}_1-\mathbf{r}_2) = \frac{e^2/\epsilon}{\sqrt{(u_1-u_2)^2+4R_+R_-\sin^2[v_1/2R_+-v_2/2R_-]+\Delta R^2}}, \tag{20}$$

where ϵ is the dielectric constant, a_z is the "thickness" of a graphene sheet, and the distance between two shells is $\Delta R=|R_+-R_-|$. In order to reduce the interaction [Eq. (17)] to an effective one-dimensional one, we use Eq. (5) and define the one-dimensional (1D) electron operators describing the slowly varying part of the electron operator $\Psi_{\beta\sigma}(\mathbf{r})$ as

$$\psi_{\beta\tilde{r}F\sigma}(u) = \frac{1}{\sqrt{2L}}\sum_q e^{i\,\text{sgn}(F)qu}c_{\beta\tilde{r}\sigma q}, \tag{21}$$

in terms of which the electron operators take the form

$$\Psi_{\beta\sigma}(\mathbf{r}) = \sum_{\tilde{r}q}\varphi^{\text{OBC}}_{\beta\tilde{r}q}(\mathbf{r})c_{\beta\tilde{r}\sigma q} = \sqrt{L}\sum_{\tilde{r}F}\text{sgn}(F)\varphi_{\beta\,\text{sgn}(F)\tilde{r}F}(\mathbf{r})\psi_{\beta\tilde{r}F\sigma}(u). \tag{22}$$

For SWCNT shells with diameter larger than ~1.5 nm, we can retain forward-scattering (or density-density) processes[21] only, such that the interacting Hamiltonian of an i-DWCNT becomes

$$H^{\text{int}}_{\text{i-DWCNT}} = \frac{1}{2}\sum_{\beta\beta'}\sum_{\tilde{r}\tilde{r}'}\sum_{FF'}\sum_{\sigma\sigma'}\int\int du_1 du_2 \rho_{\beta\tilde{r}F\sigma}(u_1) \times V^{\text{eff}}_{\beta\beta'}(u_1-u_2)\rho_{\beta'\tilde{r}'F'\sigma'}(u_2), \tag{23}$$

where $\rho_{\beta\tilde{r}F\sigma}(u)=\psi^{\dagger}_{\beta\tilde{r}F\sigma}(u)\psi_{\beta\tilde{r}F\sigma}(u)$ is the electron density operator and $V^{\text{eff}}_{\beta\beta'}$ is the effective one-dimensional Coulomb interactions obtained by using Eqs. (6) and (22),

$$V^{\text{eff}}_{\beta\beta'}(u_1,u_2) = \frac{L^2}{N_\beta N_{\beta'}}\sum_{\mathbf{R}_1\mathbf{R}_2}\int\int dv_1 dv_2 |\chi(\mathbf{r}_1-\mathbf{R}_1)|^2 \times U_{\beta\beta'}(\mathbf{r}_1-\mathbf{r}_2)|\chi(\mathbf{r}_2-\mathbf{R}_2)|^2, \tag{24}$$

where $\mathbf{R}_{1,2}$ are lattice vectors of the graphene sheet.

Let us now turn to c-DWCNTs. The total Coulomb interaction Hamiltonian of a c-DWCNT acquires a form similar to Eq. (17) when written in the basis of the bonding (antibonding) states using the transformation [Eq. (14)]. In this basis, the Coulomb interaction of a c-DWCNT is given by

$$H^{\text{int}}_{\text{c-DWCNT}} = \frac{1}{2}\sum_{\nu\nu'\sigma\sigma'}\int\int d\mathbf{r}_1 d\mathbf{r}_2 \Psi^{\dagger}_{\nu\sigma}(\mathbf{r}_1)\Psi^{\dagger}_{\nu'\sigma'}(\mathbf{r}_2) \times \tilde{U}_{\nu\nu'}(\mathbf{r}_1-\mathbf{r}_2)\Psi_{\nu'\sigma'}(\mathbf{r}_2)\Psi_{\nu\sigma}(\mathbf{r}_1), \tag{25}$$

where $\nu=\pm$ is the index for bonding and antibonding bands and the new interactions are

$$\tilde{U}_{+-} = 2\tilde{U}_{++} = 2\tilde{U}_{--} = \frac{1}{4}(U_{++}+U_{--}+U_{+-}), \tag{26}$$

where $U_{\beta\beta'}$ is defined by Eqs. (19) and (20). The electron operators in c-DWCNTs read

$$\Psi_{\nu\sigma}(\mathbf{r}) = \sum_{\tilde{r}q}\tilde{\varphi}^{\text{OBC}}_{\nu\tilde{r}q}(\mathbf{r})\tilde{c}_{\nu\tilde{r}\sigma q} = \sqrt{L}\sum_{\tilde{r}F}\text{sgn}(F)\tilde{\varphi}_{\nu\,\text{sgn}(F)\tilde{r}F}(\mathbf{r})\tilde{\psi}_{\nu\tilde{r}\sigma F}(u), \tag{27}$$

where $\tilde{\varphi}^{\text{OBC}}_{\nu\tilde{r}q}$ is the linear combination $\tilde{\varphi}^{\text{OBC}}_{\nu\tilde{r}q}(\mathbf{r})=[\varphi^{\text{OBC}}_{+\tilde{r}q}(\mathbf{r}) + \text{sgn}(\nu)\varphi^{\text{OBC}}_{-\tilde{r}q}(\mathbf{r})]/\sqrt{2}$. By using these electron operators and keeping again only the relevant forward-scattering processes, the Coulomb interaction Hamiltonian of a c-DWCNT becomes

$$H^{\text{int}}_{\text{c-DWCNT}} = \frac{1}{2}\sum_{\nu\nu'}\sum_{\tilde{r}\tilde{r}'}\sum_{FF'}\sum_{\sigma\sigma'}\int\int du_1 du_2 \tilde{\rho}_{\nu\tilde{r}F\sigma}(u_1) \times \tilde{V}^{\text{eff}}_{\nu\nu'}(u_1-u_2)\tilde{\rho}_{\nu'\tilde{r}'F'\sigma'}(u_2), \tag{28}$$

where $\tilde{\rho}_{\nu\tilde{r}F\sigma}(u)=\tilde{\psi}^{\dagger}_{\nu\tilde{r}F\sigma}(u)\tilde{\psi}_{\nu\tilde{r}F\sigma}(u)$ is the density operator and $\tilde{V}^{\text{eff}}_{\nu\nu'}$ is the effective one-dimensional Coulomb interaction,

$$\tilde{V}^{\text{eff}}_{\nu\nu'}(u_1,u_2) = \frac{L^2}{N_\nu N_{\nu'}}\sum_{\mathbf{R}_1\mathbf{R}_2}\int\int dv_1 dv_2 |\chi(\mathbf{r}_1-\mathbf{R}_1)|^2 \times \tilde{U}_{\nu\nu}(\mathbf{r}_1-\mathbf{r}_2)|\chi(\mathbf{r}_2-\mathbf{R}_2)|^2. \tag{29}$$

C. Diagonalization of the interacting Hamiltonians

In this subsection, we are going to diagonalize the interacting Hamiltonians $H_{\mathrm{DWCNT}}=H^0_{\mathrm{DWCNT}}+H^{\mathrm{int}}_{\mathrm{DWCNT}}$ for i-DWCNTs and c-DWCNTs by the use of the bosonization method.[38–41] As we are going to show, for finite size DWCNTs, the resulting Hamiltonians assume the form $H_{\mathrm{DWCNT}}=H_f+H_b$, where H_f describes the ground state and fermionic excitations, see Eqs. (31) and (32) for c-DWCNTs and i-DWCNTs, respectively, and H_b contains the bosonic excitations. Our procedure generalizes Refs. 22 and 23, where a single SWCNT shell is diagonalized, to the DWCNT case. As such for details on the bosonization procedure, we refer to Refs. 22 and 23.

First, we introduce the bosonic operators[23,31,40]

$$b_{\alpha\ \mathrm{sgn}(\tilde{r})q\sigma}=\begin{cases}\rho_{\alpha\tilde{r}q\sigma}/\sqrt{n_q} & \text{for i-DWCNTs}\\ \tilde{\rho}_{\alpha\tilde{r}q\sigma}/\sqrt{n_q} & \text{for c-DWCNTs,}\end{cases} \tag{30}$$

where $q=\pi n_q/L>0$ with n_q a positive integer and $\rho_{\alpha\tilde{r}q\sigma}$, $\tilde{\rho}_{\alpha\tilde{r}q\sigma}$ are the density operators introduced in the previous subsection. The index $\alpha=\pm$ denotes the bonding (antibonding) states in c-DWCNTs and outer (inner) shells in i-DWCNTs and we will keep this convention in the rest of the paper. The bosonic operators obey the bosonic commutation relation

$$[b_{\alpha\ \mathrm{sgn}(\tilde{r})q\sigma},b^{\dagger}_{\alpha'\ \mathrm{sgn}(\tilde{r}')q'\sigma'}]=\delta_{\alpha\alpha'}\delta_{\tilde{r}\tilde{r}'}\delta_{qq'}\delta_{\sigma\sigma'}.$$

Upon using these bosonic operators, the Hamiltonian of a DWCNT QD can be separated into its fermionic and bosonic parts, $H_{\mathrm{DWCNT}}=H_f+H_b$. For the fermionic Hamiltonian of a c-DWCNT, we find

$$H_{f,\text{c-DWCNT}}=\sum_{\alpha\tilde{r}\sigma}\frac{1}{2}\varepsilon_0\mathcal{N}^2_{\alpha\tilde{r}\sigma}+\mathrm{sgn}(\tilde{r})\Delta\varepsilon_0\mathcal{N}_{\alpha\tilde{r}\sigma}+\left(\alpha\zeta\varepsilon_0-\frac{1}{2}\varepsilon_0\right)\mathcal{N}_{\alpha\tilde{r}\sigma}+H^{\mathrm{int}}_f, \tag{31}$$

while the i-DWCNT fermionic Hamiltonian has the form

$$H_{f,\text{i-DWCNT}}=\sum_{\alpha\tilde{r}\sigma}\frac{1}{2}\varepsilon_0\mathcal{N}^2_{\alpha\tilde{r}\sigma}+\mathrm{sgn}(\tilde{r})\Delta_\alpha\varepsilon_0\mathcal{N}_{\alpha\tilde{r}\sigma}-\frac{1}{2}\varepsilon_0\mathcal{N}_{\alpha\tilde{r}\sigma}+H^{\mathrm{int}}_f. \tag{32}$$

In the above equations, H^{int}_f is the Coulomb interaction term described by

$$H^{\mathrm{int}}_f=\frac{1}{2}\sum_{\alpha\alpha'}W^{\alpha\alpha'}_{00}\left(\sum_{\tilde{r}\sigma}\mathcal{N}_{\alpha\tilde{r}\sigma}\right)\left(\sum_{\tilde{r}'\sigma'}\mathcal{N}_{\alpha'\tilde{r}'\sigma'}\right), \tag{33}$$

with the interaction strengths W_{00} obtained from

$$W^{\alpha\alpha'}_{qq}=\frac{1}{L^2}\int\int du_1du_2V^{\mathrm{eff}}_{\alpha\alpha'}(u_1-u_2)\cos(qu_1)\cos(qu_2). \tag{34}$$

Therefore, the fermionic Hamiltonian of a DWCNT QD resembles the constant-interaction model.[17]

The bosonic excitations of a DWCNT QD are described by the Hamiltonian H_b, which can be expressed in terms of the bosonic operators as

$$H_b=\sum_{q>0}\sum_{\alpha\sigma\tilde{r}}\varepsilon_0n_qb^{\dagger}_{\alpha\ \mathrm{sgn}(\tilde{r})q\sigma}b_{\alpha\ \mathrm{sgn}(\tilde{r})q\sigma}+\frac{1}{2}\sum_{q>0}\sum_{\alpha\alpha'\tilde{r}\tilde{r}'\sigma\sigma'}n_qW^{\alpha\alpha'}_{qq}(b_{\alpha\ \mathrm{sgn}(\tilde{r})q\sigma}+b^{\dagger}_{\alpha\ \mathrm{sgn}(\tilde{r})q\sigma})\times(b_{\alpha'\ \mathrm{sgn}(\tilde{r}')q\sigma'}+b^{\dagger}_{\alpha'\ \mathrm{sgn}(\tilde{r}')q\sigma'}). \tag{35}$$

In order to diagonalize the Hamiltonian H_b, we need to introduce new bosonic operators $a_{j\delta\xi q}$'s, where $j=c,s$ denote charge (spin) modes and the remaining indices $\delta=\pm$ and $\xi=\pm$ define total (relative) modes with respect to the branch and shell [or bonding (antibonding) state] degrees of freedoms, respectively. The new bosonic operators are related to the bosonic operators $b_{\alpha\ \mathrm{sgn}(\tilde{r})q\sigma}$ by a Bogoliubov transformation[31,42]

$$b_{\alpha\ \mathrm{sgn}(\tilde{r})q\sigma}=\sum_{j\delta\xi}\Lambda^{j\delta\xi}_{\alpha\tilde{r}\sigma}(q)(S_{j\delta\xi q}a_{j\delta\xi q}+C_{j\delta\xi q}a^{\dagger}_{j\delta\xi q}), \tag{36}$$

where the coefficient matrix is given by

$$\Lambda^{j\delta\xi}_{\alpha\tilde{r}\sigma}(q)=\frac{1}{2\sqrt{2}}\begin{pmatrix}\sin\theta_q+\cos\theta_q & -\cos\theta_q+\sin\theta_q & 1 & 1 & 1 & 1 & 1 & 1\\ \sin\theta_q+\cos\theta_q & -\cos\theta_q+\sin\theta_q & 1 & 1 & -1 & -1 & -1 & -1\\ \sin\theta_q+\cos\theta_q & -\cos\theta_q+\sin\theta_q & -1 & -1 & 1 & 1 & -1 & -1\\ \sin\theta_q+\cos\theta_q & -\cos\theta_q+\sin\theta_q & -1 & -1 & -1 & -1 & 1 & 1\\ \sin\theta_q+\cos\theta_q & -\cos\theta_q-\sin\theta_q & 1 & -1 & 1 & -1 & 1 & -1\\ \sin\theta_q+\cos\theta_q & -\cos\theta_q-\sin\theta_q & 1 & -1 & -1 & 1 & -1 & 1\\ \sin\theta_q+\cos\theta_q & -\cos\theta_q-\sin\theta_q & -1 & 1 & 1 & -1 & -1 & 1\\ \sin\theta_q+\cos\theta_q & -\cos\theta_q-\sin\theta_q & -1 & 1 & -1 & 1 & 1 & -1\end{pmatrix}, \tag{37}$$

and for the matrix elements we use the ordering $j\delta\xi = c++, c+-, c-+, c--, s++, s+-, s-+, s--$ and $\alpha\tilde{r}\sigma = +\tilde{R}\uparrow, +\tilde{R}\downarrow, +\tilde{L}\uparrow, +\tilde{L}\downarrow, -\tilde{R}\uparrow, -\tilde{R}\downarrow, -\tilde{L}\uparrow, -\tilde{L}\downarrow$. The q dependence of the matrix is in the trigonometric functions

$$\sin\theta_q = |W_{qq}^{++} - W_{qq}^{--}|/\{(W_{qq}^{++} - W_{qq}^{--})^2 + [W_{qq}^{+-} + \sqrt{(W_{qq}^{++} - W_{qq}^{--})^2 + (W_{qq}^{+-})^2}]^2\}^{1/2}.$$

The remaining coefficients are

$$S_{j\delta\xi q} = 1 \quad \text{and} \quad C_{j\delta\xi q} = 0, \tag{38}$$

in the cases $(j\delta\xi) = (c-\pm), (s\pm\pm)$, i.e., for the relative (with respect to the branch index) charge modes and for all of the spin modes. For the total and relative (with respect to the shell or band index) charge modes $(c+\pm)$, the two coefficients are interaction dependent,

$$S_{c+\pm q} = \frac{1}{2}\left[\sqrt{\frac{\varepsilon_0}{\varepsilon_{c+\pm}(q)}} + \sqrt{\frac{\varepsilon_{c+\pm}(q)}{\varepsilon_0}}\right],$$

$$C_{c+\pm q} = \frac{1}{2}\left[\sqrt{\frac{\varepsilon_0}{\varepsilon_{c+\pm}(q)}} - \sqrt{\frac{\varepsilon_{c+\pm}(q)}{\varepsilon_0}}\right], \tag{39}$$

where

$$\varepsilon_{c+\pm}(q) = \varepsilon_0\sqrt{1 + 8W_{qq}^{\pm\pm}/\varepsilon_0} \tag{40}$$

are the energies of the total and relative charge modes. The interactions do not affect the six "neutral" modes, $(j\delta\xi) = (c-\pm), (s\pm\pm)$, and their energy dispersions are the same as for the noninteracting system,

$$\varepsilon_{j\delta\xi}(q) = \varepsilon_0. \tag{41}$$

By using the new bosonic operators, the excitation Hamiltonian assumes finally the diagonal form

$$H_b = \sum_{q>0}\sum_{j\delta\xi} \varepsilon_{j\delta\xi}(q) a_{j\delta\xi q}^\dagger a_{j\delta\xi q}, \tag{42}$$

and its eigenstates are

$$|\mathbf{N},\mathbf{m}\rangle := \prod_{q>0}\prod_{j\delta\xi} \frac{1}{\sqrt{m_{j\delta\xi q}!}} (a_{j\delta\xi q}^\dagger)^{m_{j\delta\xi q}} |\mathbf{N},\mathbf{0}\rangle, \tag{43}$$

where $\mathbf{N} = \{N_{\alpha\tilde{r}\sigma}\}$ defines the number of electrons in each of the eight branches $(\alpha\tilde{r}\sigma)$ and $\mathbf{m} = \{m_{j\delta\xi q}\}$ describes the configuration of the bosonic excitations in each of the eight modes $(j\delta\xi)$. The state $|\mathbf{N},\mathbf{0}\rangle$ contains no bosonic excitations and describes the ground state or the fermionic excited states of the Hamiltonians H_f in Eqs. (31) and (32).

III. DYNAMICS OF THE DOUBLE-WALLED CARBON NANOTUBE QUANTUM DOT SYSTEM

The transport properties of the DWCNT QD system can be obtained by investigating the dynamics of its density matrix.[43] In this section, we briefly show how to derive the equation of motion for the reduced density matrix of the DWCNT QD system. By solving these equations, we obtain the stationary current through the system when a bias voltage is applied.

A. Equation of motion for the reduced density matrix

As we consider a very weak coupling between the DWCNT and the two leads, the tunneling Hamiltonian can be treated as a perturbation. This means that higher order tunneling processes as cotunneling or correlated sequential tunneling are neglected.[44] We start from the equation for motion for the density matrix in the interaction picture,[43]

$$i\hbar\frac{\partial\rho_{\text{tot}}^I(t)}{\partial t} = [H_T^I(t), \rho_{\text{tot}}^I(t)], \tag{44}$$

where $\rho_{\text{tot}}^I(t)$ is the density matrix of the whole system (including the DWCNT and the leads) and the tunneling Hamiltonian in the interaction picture is

$$H_T^I(t) = e^{(i/\hbar)(H_{\text{DWCNT}}+H_{\text{leads}})(t-t_0)} H_T e^{-(i/\hbar)(H_{\text{DWCNT}}+H_{\text{leads}})(t-t_0)}. \tag{45}$$

This equation can be solved formally as

$$\rho_{\text{tot}}^I(t) = \rho_{\text{tot}}^I(t_0) - \frac{i}{\hbar}\int_{t_0}^t dt_1 [H_T^I(t_1), \rho_{\text{tot}}^I(t_1)]. \tag{46}$$

Substituting the above expression of $\rho_{\text{tot}}^I(t)$ back to Eq. (44), we have

$$\frac{\partial\rho_{\text{tot}}^I(t)}{\partial t}(t) = -\frac{i}{\hbar}[H_T^I(t), \rho_{\text{tot}}^I(t_0)] + \left(\frac{i}{\hbar}\right)^2 \int_{t_0}^t dt_1 [H_T^I(t), [H_T^I(t_1), \rho_{\text{tot}}^I(t_1)]]. \tag{47}$$

As we are only interested in the transport through the DWCNT QD, we will focus on the reduced density matrix of the QD which is obtained by tracing out the degrees of freedom of the leads,

$$\rho^I = \text{Tr}_{\text{leads}}\{\rho_{\text{tot}}^I\}. \tag{48}$$

Because the leads are very large compared with the DWCNT and the tunneling events between leads and the QD are rare, the effect of the DWCNT on the leads can be ignored and the leads can be described as reservoirs remaining in thermal equilibrium. We use the ansatz[23] to factorize the total density matrix $\rho^I(t)$,

$$\rho_{\text{tot}}^I(t) = \rho_{\text{leads}}^I \rho^I(t) = \rho_s^I \rho_d^I \rho^I(t), \tag{49}$$

where the density matrix of the leads ρ_{leads} is time independent and is described by the thermal equilibrium distribution,

$$\rho_{s/d}^I = \frac{e^{-\beta(H_{s/d}-\mu_{s/d}N_{s/d})}}{\text{Tr}\{e^{-\beta(H_{s/d}-\mu_{s/d}N_{s/d})}\}},$$

where $\mu_{s/d}$ is the chemical potential of the source/drain lead and $\beta = 1/k_B T$. We further simplify Eq. (47) by introducing the Markov approximation, that is, we assume that $\dot{\rho}_{\text{tot}}^I(t)$ depends on $\rho_{\text{tot}}^I(t)$ only and replace $\rho_{\text{tot}}^I(t')$ by $\rho_{\text{tot}}^I(t)$. By using the Markov approximation, we effectively neglect the details of the dynamics of $\rho_{\text{tot}}^I(t)$ at short time scales. Since we are interested in the dc, i.e., in the dynamics at long time scales, this approximation is legitimate.

We make the further assumptions that the elements of the reduced density matrix between two states with different charges vanish and that the elements between two nondegenerate states with same charges also vanish.[22,23] Finally, the master equations of the reduced density matrix can be expressed in Bloch-Redfield form[45,46]

$$\dot{\rho}_{nm}^{I,E_N}(t) = -\sum_{kk'} R_{nmkk'}^{E_N} \rho_{kk'}^{I,E_N}(t) + \sum_{M=N\pm1} \sum_{E'} \sum_{kk'} R_{nmkk'}^{E_N E'_M} \rho_{kk'}^{I,E'_M}(t), \tag{50}$$

where n, m, k, and k' are indices of the eigenstates of the DWCNT Hamiltonian. The Redfield tensors are defined as

$$R_{nmkk'}^{E_N} = \sum_{l} \sum_{M,E',j} (\delta_{mk'} \Gamma_{l,njjk}^{(+)E_N E'_M} + \delta_{nk} \Gamma_{l,k'jjm}^{(-)E_N E'_M}), \tag{51}$$

$$R_{nmkk'}^{E_N E'_M} = \sum_{l} \Gamma_{l,k'mnk}^{(+)E'_M E_N} + \Gamma_{l,k'mnk}^{(-)E'_M E_N}, \tag{52}$$

where the transition rates $\Gamma^{(\pm)}$ depend on the properties of the contacts between the leads and the DWCNT QD.[23] For typical normal metal contacts, it is justified to assume that the contacts do not mix the electrons in the different branches and that the couplings between the leads and the DWCNT do not depend on either the wave vectors or the spins of the tunneling electrons. Then, as shown in Appendix B, the transition rates for tunneling onto the dot depend on the energy of the tunneling electrons as

$$\Gamma_{l,k'mnk}^{(\pm)E_N E'_{N+1}} = \sum_{\alpha} \frac{4\pi CL}{N_\alpha \hbar^2} \sum_{\mathbf{R}p} |T_{l\alpha}(\mathbf{x}_{\mathbf{R},p})|^2 \int d\varepsilon g_l(\varepsilon) f(\varepsilon) \times \int_0^\infty dt' e^{\pm(i/\hbar)(\varepsilon - eV_l - E'_{N+1} + E_N)t'} \times \sum_{\tilde{r}\sigma F} [\psi_{\alpha\tilde{r}\sigma F}(u_l)]_{k'm}^{E_N E'_{N+1}} [\psi_{\alpha\tilde{r}\sigma F}^\dagger(u_l)]_{nk}^{E'_{N+1} E_N}, \tag{53}$$

where we introduced the matrix elements of the 1D operators between the states $|m\rangle$, $|k'\rangle$ and between $|n\rangle$, $|k\rangle$. The functions $g_l(\varepsilon)$ and $f(\varepsilon)$ denote the density of states of lead l and the Fermi function, respectively. Finally, C is a constant coming from the integration over the p_z orbitals, L is the tube length, N_α is the total electron number in shell (band) α, and $T_{l\alpha}(\mathbf{x})$ comes from the tunneling Hamiltonian. The eigenstates involved in the tunneling processes are [cf. Eq. (43) for the expression of the DWCNT eigenstates]

$$|k'\rangle = |\mathbf{N}, \mathbf{k}'\rangle, \quad |m\rangle = |\mathbf{N}+\mathbf{1}, \mathbf{m}\rangle,$$

$$|n\rangle = |\mathbf{N}+\mathbf{1}, \mathbf{n}\rangle, \quad |k\rangle = |\mathbf{N}, \mathbf{k}\rangle.$$

Similarly, the expressions for the tunneling rates out of the dot are

$$\Gamma_{l,k'mnk}^{(\pm)E_N E'_{N-1}} = \sum_{\alpha} \frac{4\pi CL}{N_\alpha \hbar^2} \sum_{\mathbf{R}p} |T_{l\alpha}(\mathbf{x}_{\mathbf{R},p})|^2 \int d\varepsilon g_l(\varepsilon)(1 - f(\varepsilon)) \times \int_0^\infty dt' e^{\mp(i/\hbar)(\varepsilon - eV_l + E'_{N-1} - E_N)t'} \times \sum_{\tilde{r}\sigma F} [\psi_{\alpha\tilde{r}\sigma F}^\dagger(u_l)]_{k'm}^{E_N E'_{N-1}} [\psi_{\alpha\tilde{r}\sigma F}(u_l)]_{nk}^{E'_{N-1} E_N}, \tag{54}$$

with the eigenstates

$$|k'\rangle = |\mathbf{N}, \mathbf{k}'\rangle, \quad |m\rangle = |\mathbf{N}-\mathbf{1}, \mathbf{m}\rangle,$$

$$|n\rangle = |\mathbf{N}-1, \mathbf{n}\rangle, \quad |k\rangle = |\mathbf{N}, \mathbf{k}\rangle.$$

B. Calculation of the current

We are only interested in the properties of the system in the stationary state, which can be obtained by solving Eq. (50) with the left hand side set to be zero. The current can be calculated by using the tunneling rates between the DWCNT QD and the leads. The current measured in experiments is the current in one lead, which can be calculated as

$$I_l = e \sum_N (\Theta_l^{N\to N+1} - \Theta_l^{N\to N-1}), \tag{55}$$

where $\Theta_l^{N\to N\pm1}$ are the tunneling rates between the QD and the lead l when the particle number in the DWCNT QD changes from N to $N\pm1$. The tunneling rates are related to the transition rates and the reduced density matrix as

$$\Theta_l^{N\to N\pm1} = \sum_{E,E'} \sum_{nkj} (\Gamma_{l,njjk}^{(+)E_N E'_{N\pm1}} \rho_{kn}^{I,E_N} + \rho_{nk}^{I,E_N} \Gamma_{l,kjjn}^{(-)E_N E'_{N\pm1}}). \tag{56}$$

After substituting Eq. (56) into Eq. (55), the current can be expressed in terms of the transition rates and the elements of the reduced density matrix as

$$I_l = e \sum_{N,E,E'} (\Gamma_{l,njjk}^{(+)E_N E'_{N+1}} - \Gamma_{l,njjk}^{(+)E_N E'_{N-1}}) \rho_{kn}^{I,E_N} + (\Gamma_{l,kjjn}^{(-)E_N E'_{N+1}} - \Gamma_{l,kjjn}^{(-)E_N E'_{N-1}}) \rho_{nk}^{I,E_N}. \tag{57}$$

IV. LINEAR AND NONLINEAR TRANSPORT

After having obtained the energy spectrum and the eigenstates of the DWCNT QD system, we can calculate the transition rates, Eqs. (53) and (54), and use the Bloch-Redfield equations for the reduced density matrix to calculate the transport properties of the system. Here, we present the calculated results of both linear and nonlinear conductances.

A. Linear conductance

In the linear transport regime, i.e., $|eV_b| \ll k_B T \ll \varepsilon_0$, where V_b is the applied bias, only the ground states with N and $N+1$ electrons are involved in the transport. In this case, the equations for the diagonal elements and the off-diagonal el-

ements of the reduced density matrix are decoupled from each other[23] and we only have to take into account the diagonal elements of the ground states with a certain electron number, which are the occupation probabilities. In this case, only the real part of the rates $\Gamma^{(\pm)}_{l,knnk}$ enters the Bloch-Redfield equation [Eq. (50)]. Moreover, since no bosonic excitations are present, the rates reduce to the very simple expressions, cf. Eqs. (B14) and (B15),

$$\Gamma^{\text{in}}_{l,kn} := \Re(\Gamma^{(\pm)E_N E'_{N+1}}_{l,knnk}) = \sum_{\alpha\tilde{r}\sigma} \frac{\gamma_{l\alpha}(\varepsilon_l)}{h} f(\varepsilon_l)\, \delta_{\mathbf{N}+\mathbf{e}_{\alpha\tilde{r}\sigma},\mathbf{N}+\mathbf{1}}, \tag{58}$$

with the eigenstates $|k\rangle = |\mathbf{N},\mathbf{0}\rangle$, $|n\rangle = |\mathbf{N}+\mathbf{1},\mathbf{0}\rangle$ and with $\varepsilon_l = eV_l + E'_{N+1} - E_N$. Analogously,

$$\Gamma^{\text{out}}_{l,kn} := \Re(\Gamma^{(\pm)E_N E'_{N-1}}_{l,knnk}) = \sum_{\alpha\tilde{r}\sigma} \frac{\gamma_{l\alpha}(\varepsilon'_l)}{h} [1 - f(\varepsilon'_l)]\, \delta_{\mathbf{N}-\mathbf{e}_{\alpha\tilde{r}\sigma},\mathbf{N}-\mathbf{1}}, \tag{59}$$

with the eigenstates $|k\rangle = |\mathbf{N},\mathbf{0}\rangle$ $|n\rangle = |\mathbf{N}-\mathbf{1},\mathbf{0}\rangle$ and with $\varepsilon'_l = eV_l - E'_{N-1} + E_N$. Moreover, we introduced the rate function

$$\gamma_{l\alpha}(\varepsilon) = \frac{8\pi^3 C g_l(\varepsilon) W^2(u_l)}{N_\alpha} \sum_{\mathbf{R}p} |T_{l\alpha}(\mathbf{x}_{\mathbf{R},p})|^2.$$

As shown in Appendix B, the function $W(u)$ accounts for a nonoscillatory spatial dependence due to the Coulomb interaction. The stationary occupation probability of the ground state with N electrons can now be easily evaluated. We find, see also Ref. 23,

$$P_N = \frac{\sum_{l\alpha} \gamma_{l\alpha}[1 - f(\varepsilon_l)] C^\alpha_{N+1,N}}{\sum_{l\alpha} \gamma_{l\alpha} f(\varepsilon_l) C^\alpha_{N,N+1} + \gamma_{l\alpha}[1 - f(\varepsilon_l)] C^\alpha_{N+1,N}}, \tag{60}$$

where $C^\alpha_{N,N+1}$ are the number of permitted ground states with $N+1$ particles when one electron is added to a ground state with N particles, and this electron is added to the bonding (antibonding) state α in c-DWCNTs or to the shell α in i-DWCNTs. We define the energy $\varepsilon_l = eV_l - \Delta E$ and the energy difference $\Delta E = E^0_N - E^0_{N+1} - \mu_g$, where μ_g is the electrochemical potential in the gate. The linear conductance is then given as

$$G = \frac{e^2\beta}{h} \frac{\sum_\alpha \gamma_{s\alpha}\gamma_{d\alpha} C^\alpha_{N,N+1} C^\alpha_{N+1,N}}{\sum_{l\alpha} \gamma_{l\alpha} f(-\Delta E) C^\alpha_{N,N+1} + \gamma_{l\alpha}[1 - f(-\Delta E)] C^\alpha_{N+1,N}} \frac{e^{-\beta\Delta E}}{(1 + e^{-\beta\Delta E})^2}, \tag{61}$$

where we assume that the bias is symmetrically applied to the source and drain leads, that is, $-V_s = V_d = V_b/2$. The maximum value of the linear conductance is

$$G_{\max} = \frac{e^2\beta}{h} \frac{\sum_\alpha \gamma_{s\alpha}\gamma_{d\alpha} C^\alpha_{N,N+1} C^\alpha_{N+1,N}}{\sum_{l\alpha} \gamma_{l\alpha}(C^\alpha_{N,N+1} + C^\alpha_{N+1,N}) + 2\sqrt{\left(\sum_{l\alpha} \gamma_{l\alpha} C^\alpha_{N,N+1}\right)\left(\sum_{l\alpha} \gamma_{l\alpha} C^\alpha_{N+1,N}\right)}}. \tag{62}$$

and the maxima of the conductance as a function of μ_g are at $-\mu_g = E^0_{N+1} - E^0_N + \Delta E_{\max}$, where[18,22,23,48,49]

$$\Delta E_{\max} = \frac{1}{2\beta} \ln \frac{\sum_{l\alpha} \gamma_{l\alpha} C^\alpha_{N+1,N}}{\sum_{l\alpha} \gamma_{l\alpha} C^\alpha_{N,N+1}}. \tag{63}$$

The conductance peak occurs whenever an electron is added or removed from the DWCNT QD by changing the electrochemical potential in the gate. At zero temperature, from Eq. (63), $\Delta E_{\max}$ vanishes and the conductance peak occurs when the electrochemical potential of the gate satisfies the following condition:

$$-\mu_g = E^0_{N+1} - E^0_N \equiv \mu_N.$$

Therefore, at zero temperature, the addition energy $\delta\mu_N$ is given by

$$\delta\mu_N = |\mu_N - \mu_{N-1}| = |E^0_{N+1} + E^0_{N-1} - 2E^0_N|.$$

For a c-DWCNT QD system, electrons can tunnel into both shells because of nonzero intershell couplings. Hence, there is an eight-electron periodicity of the conductance peak distances,

$$\delta\mu_1 = \delta\mu_3 = \delta\mu_5 = \delta\mu_7 = W^{++}_{00}, \tag{64}$$

$$\delta\mu_2 = \delta\mu_6 = 2\min(\Delta,\zeta)\varepsilon_0 + W^{++}_{00}, \tag{65}$$

$$\delta\mu_4 = 2|\Delta - \zeta|\varepsilon_0 + W^{++}_{00}, \tag{66}$$

$$\delta\mu_8 = \varepsilon_0 - 2(\Delta + \zeta)\varepsilon_0 + W^{++}_{00}. \tag{67}$$

Here, we use the relation $W^{++}_{00} = W^{--}_{00} = W^{+-}_{00}/2$ in c-DWCNTs [cf. Eq. (26)]. On the other hand, electrons can only tunnel into the outer shell in an i-DWCNT QD system because the contacts are deposited onto the outer shell and the intershell

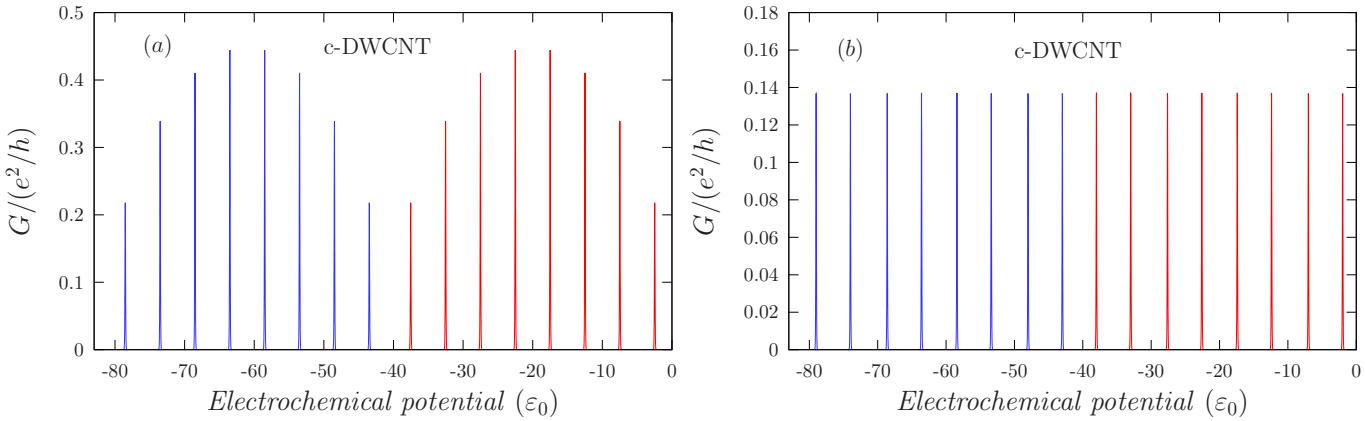

FIG. 5. (Color online) Calculated linear conductances as a function of the gate electrochemical potential in c-DWCNT QD systems with different parameters. (a) $\Delta=\zeta=0.0$, $W_{00}^{++}=W_{00}^{--}=W_{00}^{+-}/2=5.0\varepsilon_0$, and $k_BT=0.025\varepsilon_0$, where the level spacing ε_0 is used as the unit of energy. The coupling strengths are $\gamma_{s\pm}=\gamma_{d\pm}=0.02\varepsilon_0$. (b) $\Delta=0.2$ and $\zeta=0.3$. The remaining parameters are the same as those in (a). In both cases, the linear conductances in c-DWCNTs show an eight-electron periodicity. In the case of zero mismatch parameters shown in (a), an eight-electron periodicity of the heights of the conductance peaks also occurs. For finite mismatch shown in (b), the peak heights are equal but the eight-electron periodicity of the addition energies, i.e., the peak distances, remains (to emphasize this, we assign to each group of eight peaks different colors).

couplings vanish. Therefore, there is a four-electron periodicity of the conductance peak distance like in a SWCNT QD system,

$$\delta\mu_1 = \delta\mu_3 = W_{00}^{++}, \tag{68}$$

$$\delta\mu_2 = 2\Delta_+\varepsilon_0 + W_{00}^{++}, \tag{69}$$

$$\delta\mu_4 = \varepsilon_0 - 2\Delta_+\varepsilon_0 + W_{00}^{++}. \tag{70}$$

Because electrons tunnel only into the outer shell with the interaction strength W_{00}^{++}, the addition energy $\delta\mu_N$ does not depend either on the interaction strength in the inner shell W_{00}^{--} or on the intershell interaction strength W_{00}^{+-}. Information on these Coulomb interactions is in the bosonic part of the excitation spectrum seen at higher energies, cf. Eq. (40), and in the matrix elements of the electron operators.

The calculated linear conductances of DWCNT QDs of different configurations are shown in Figs. 5 and 6. In a c-DWCNT QD, the intraband interaction strengths W_{00}^{++} and W_{00}^{--} are the same, while the interband interaction strength W_{00}^{+-} is twice as large [cf. Eq. (26)]. However, in an i-DWCNT, the interaction strength in the inner shell W_{00}^{--} is the strongest because of the smaller inner shell radius and one has $W_{00}^{--}>W_{00}^{+-}>W_{00}^{++}$. The shapes of the conductance peaks strongly depend on the mismatch parameters, i.e., Δ and ζ in c-DWCNTs and $\Delta_\pm$ in i-DWCNTs. For zero mismatch parameters, the quantities $C_{N,N+1}^{\alpha}$ and $C_{N+1,N}^{\alpha}$ are $C_{N,N+1}^{\alpha}=4,3,2,1$ and $C_{N+1,N}^{\alpha}=1,2,3,4$ for $N^{\alpha}=4m,4m$

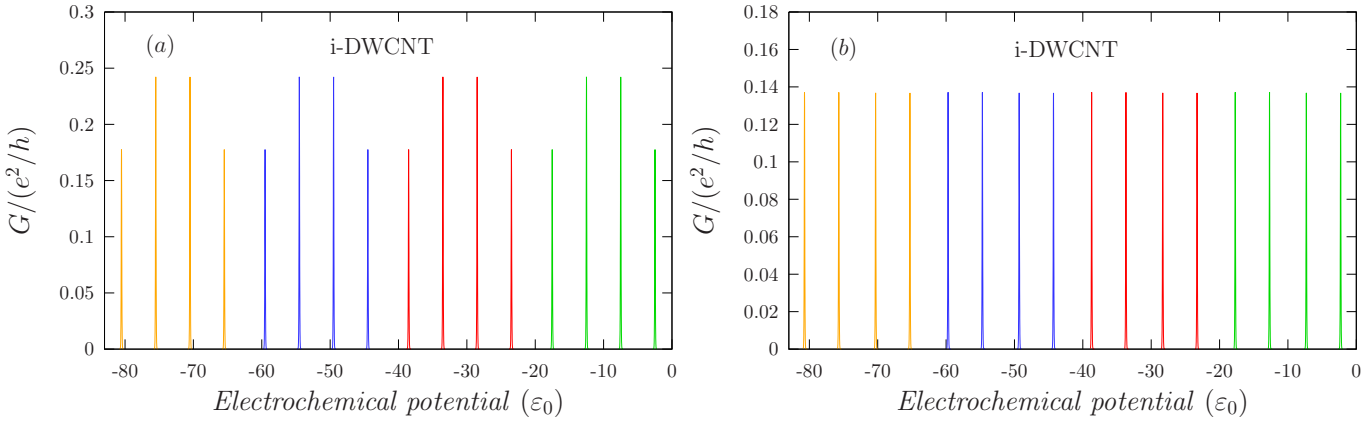

FIG. 6. (Color online) Calculated linear conductances as a function of the gate electrochemical potential in i-DWCNT QD systems with different parameters. (a) $\Delta_+=\Delta_-=0.0$, $W_{00}^{++}=5\varepsilon_0$, $W_{00}^{--}=6.0\varepsilon_0$, $W_{00}^{+-}=5.5\varepsilon_0$, and $k_BT=0.025\varepsilon_0$, where the level spacing ε_0 is used as the unit of energy. The coupling strengths are $\gamma_{s+}=\gamma_{d+}=0.02\varepsilon_0$ and $\gamma_{s-}=\gamma_{d-}=0$. (b) $\Delta_+=0.2$ and $\Delta_-=0.3$. The remaining parameters are the same as those in (a). The linear conductances in i-DWCNTs show a four-electron periodicity. In the absence of mismatch shown in (a), the four-electron periodicity is observed also in the peak heights, while it is no longer observed at finite mismatch shown in (b). However, the addition energy, i.e., the peak distance, shows a four-electron periodicity in both cases (to emphasize this, we assign to each group of four peaks different colors).

$+1,4m+2,4m+3$ with an integer m, where N^α is the electron number either in the bonding (antibonding) state α in c-DWCNTs or in the shell α in i-DWCNTs. Therefore, according to Eq. (62), one can find that the conductance peak heights show an eight-electron periodicity in a c-DWCNT QD [cf. Fig. 5(a)] because both bonding and antibonding states contribute to the electron transport. However, there is a four-electron periodicity in an i-DWCNT QD [cf. Fig. 6(a)] because only the outer shell contributes. If the mismatch parameters are nonzero, we find $C^\alpha_{N,N+1}=2,1,2,1$ and $C^\alpha_{N+1,N}=1,2,1,2$ for $N^\alpha=4m,4m+1,4m+2,4m+3$. Therefore, all the conductance peaks have the same heights [cf. Figs. 5(b) and 6(b)]. However, the distance between two conductance peaks, i.e., the addition energy, always shows an eight-electron periodicity in c-DWCNT QDs and the four-electron periodicity in i-DWCNTs, as shown in the Figs. 5 and 6. For c-DWCNTs, the parameters W_{00}'s, $\min(\Delta,\zeta)$, $\max(\Delta,\zeta)$, and ε_0 can be determined by experimentally measuring the distances of the conductance peaks. The exact values of Δ and ζ cannot be obtained because their exact values determine the way how one by one electrons fill in the bonding and antibonding bands, which cannot be probed by measuring the conductances only. The parameters W^{++}_{00}, Δ_+, and ε_0 of i-DWCNTs can also be determined by fitting the experimental results for the conductance.

B. Nonlinear conductances

When higher bias is applied, i.e., $|eV_b| \geqslant \varepsilon_0 \gg k_BT$, we can only solve the Bloch-Redfield equations numerically. For the elastic tunneling process, we have to include the coherences between the states with same particle number **N** but with different bosonic excitations **m**.[22,23] Because of the large number of degenerate bosonic excitations, the rank of the reduced density matrix increases very fast as the applied bias increases, which causes a very long computing time to solve the equations. On the other hand, these coherences can be ignored in an inelastic tunneling process, in which the QD system will be restored to the equilibrium states before the next tunneling process. Only the diagonal elements in the reduced density matrix are nonzero and they obey the Boltzmann distribution as

$$\rho^{I,E_N}_{nn}(t) = \mathcal{P}_N(t)\frac{e^{-\beta E^n_N}}{\sum_k e^{-\beta E^k_N}},$$

where n and k are indices of the eigenstates of the DWCNT QD Hamiltonian and $\mathcal{P}_N(t)$ is the probability of finding N electrons in the QD. Instead of solving the Bloch-Redfield equations directly, we can solve the equation of motion for the probability $\mathcal{P}_N(t)$,

$$\frac{d}{dt}\mathcal{P}_N(t) = -\sum_{l,M=N\pm1}\Theta^{N\to M}_l + \sum_{l,M=N\pm1}\Theta^{M\to N}_l, \qquad (71)$$

where the tunneling rate is defined in Eq. (56) and can now be expressed in terms of $\mathcal{P}_N(t)$ as

$$\Theta^{N\to N\pm1}_l = \mathcal{P}_N(t)\sum_{E,E'}\frac{e^{-\beta E^n_N}}{\sum_k e^{-\beta E^k_N}}\left(\sum_{nj}\Gamma^{(+)E_N E'_{N\pm1}}_{l,njjn} + \Gamma^{(-)E_N E'_{N\pm1}}_{l,njjn}\right). \qquad (72)$$

The number of the equations reduces significantly; we can solve them quite fast. In Fig. 7, we show the calculated stability diagram of a DWCNT QD system in an inelastic tunneling process. The size of the Coulomb diamonds shows an eight-electron periodicity in c-DWCNT QDs and a four-electron periodicity in i-DWCNT QDs. The excitation lines are also shown in Fig. 7, which contain contributions of both fermionic [cf. Eqs. (31) and (32)] and bosonic excitations [cf. Eq. (42)]. There are more excitation lines in c-DWCNT QDs than in i-DWCNT QDs because of the larger number of the ground states of c-DWCNTs. The stability diagram of an i-DWCNT QD looks quite similar to that of a SWCNT QD, which also shows a four-electron periodicity. However, the configurations of the excitation lines of the two cases are different because the excitation spectrum in i-DWCNTs contains an extra contribution from the Coulomb interaction due to the electrons in the inner shell.

V. CONCLUSIONS

In this paper, we consider QD systems formed by finite length c-DWCNTs and i-DWCNTs with two metallic shells. The energy spectrum of the systems is calculated under open boundary conditions. The transport properties of the DWCNT QD system are obtained by solving the Bloch-Redfield equations for the reduced density matrix of the system. Because the contacts are usually deposited on the outer shell and the intershell coupling depends on the chiralities of the two shells, we find an eight-electron periodicity of the linear conductance peak distances in c-DWCNTs but a four-electron periodicity in i-DWCNTs. The peak heights strongly depend on the degeneracies of the ground states. By including both fermionic and bosonic excitations, we also calculate the stability diagrams of QD systems with both c-DWCNTs and i-DWCNTs in an inelastic tunneling process. The periodicity of the Coulomb diamond sizes depends on the number of the shells contributing to the electron transport. Therefore, the four-electron periodicity in a MWCNT QD measured in the experiments in Ref. 28 may be due to the fact that only the outermost metallic shell was involved in the electron transport. For a DWCNT QD with a metallic outer shell and a semiconducting inner one, the distances of the linear conductance peaks will also show a four-electron periodicity since the inner semiconducting shell does not contribute to the electron transport. Similarly, the four-electron periodicity in i-DWCNTs is because of the negligible intershell coupling and there will be an eight-electron periodicity if a large intershell coupling is caused, for example, by contacts. Therefore, it is necessary to use properly prepared contacts in order to observe the different periodicities of Coulomb blockade oscillations in different types of DWCNTs in the experiments.

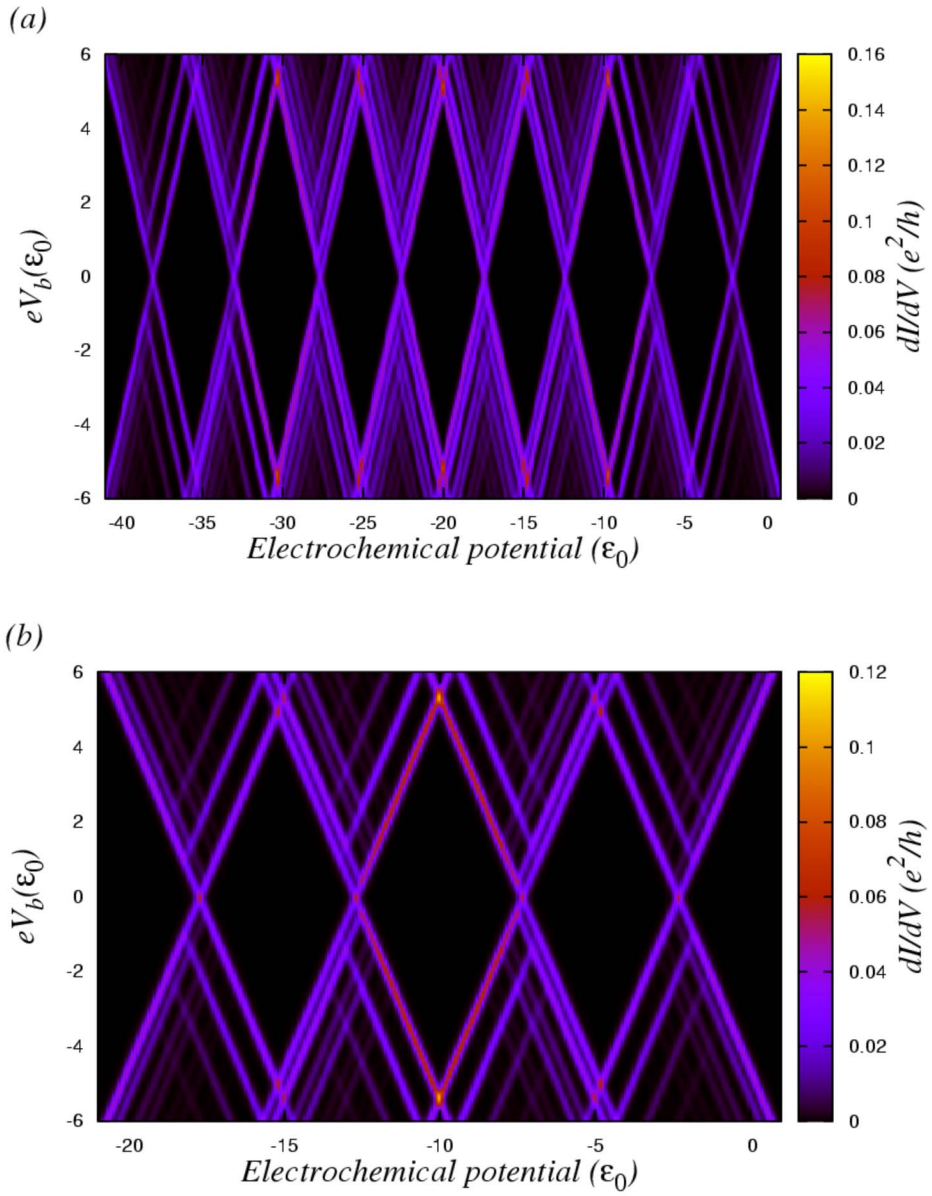

FIG. 7. (Color online) Calculated stability diagrams of DWCNT QD systems. (a) Stability diagram of a c-DWCNT QD. The parameters are $\Delta=0.2$, $\zeta=0.3$, $W_{00}^{+}=W_{00}^{-}=W_{00}^{+-}/2=5.0\varepsilon_0$, and $k_BT=0.05\varepsilon_0$, where the level spacing ε_0 is used as the unit of energy. We use $\gamma_{s\pm}=\gamma_{d\pm}=0.02\varepsilon_0$ for the coupling strengths between the leads and the DWCNT QD. (b) Stability diagram of an i-DWCNT QD. The parameters are $\Delta_+=0.2$, $\Delta_-=0.3$, $W_{00}^{+}=5\varepsilon_0$, $W_{00}^{-}=6.0\varepsilon_0$, $W_{00}^{+-}=5.5\varepsilon_0$, and $k_BT=0.05\varepsilon_0$. The coupling strengths are $\gamma_{s+}=\gamma_{d+}=0.02\varepsilon_0$ and $\gamma_{s-}=\gamma_{d-}=0$. The size of the Coulomb diamonds shows an eight-electron periodicity in c-DWCNT QDs, as shown in (a), while it shows a four-electron periodicity in i-DWCNT QDs, as shown in (b).

ACKNOWLEDGMENTS

The authors would like to thank L. Mayrhofer for helpful discussions. The authors acknowledge the support of DFG under the program GRK 638.

APPENDIX A: MATRIX ELEMENTS OF THE ELECTRON OPERATORS

In this appendix, we calculate the matrix elements of the electron operators [Eqs. (22) and (27)] in the basis of the eigenstates [Eq. (43)] of the Hamiltonian H_{DWCNT} and the results are used in Sec. III. The matrix elements of the electron operator are calculated by using the relation

$$\langle \mathbf{N},\mathbf{m}|\Psi_{\alpha\sigma}(\mathbf{r})|\mathbf{N}',\mathbf{m}'\rangle = \sqrt{L}\sum_{\tilde{r}F} \mathrm{sgn}(F)\varphi_{\alpha\ \mathrm{sgn}(F)\tilde{r}F}(\mathbf{r}) \times \langle \mathbf{N},\mathbf{m}|\psi_{\alpha\tilde{r}F\sigma}(u)|\mathbf{N}',\mathbf{m}'\rangle. \quad \text{(A1)}$$

The 1D electron operator $\psi_{\alpha\tilde{r}F\sigma}$ can be expressed in terms of the bosonic operators introduced above as[39,40]

$$\psi_{\alpha\tilde{r}F\sigma}(u) = \frac{\eta_{\alpha\tilde{r}\sigma}K_{\alpha\tilde{r}F\sigma}(u)}{\sqrt{1-e^{-a\pi/L}}} e^{i\phi^{\dagger}_{\alpha\tilde{r}F\sigma}(u)+i\phi_{\alpha\tilde{r}F\sigma}(u)}, \quad \text{(A2)}$$

where a is an infinitesimal positive number used to avoid the divergence in the long wavelength limit and the operator $\eta_{\alpha\tilde{r}\sigma}$ is the Klein factor, which destroys a particle in the branch $\alpha\tilde{r}\sigma$ when acting on the eigenstates of the DWCNT Hamiltonian,

$$\eta_{\alpha\tilde{r}\sigma}|\mathbf{N},\mathbf{m}\rangle = (-1)^{\sum_{i=1}^{\alpha\tilde{r}\sigma-1}N_i}|\mathbf{N}-\mathbf{e}_{\alpha\tilde{r}\sigma},\mathbf{m}\rangle,$$

where we use the convention $i=+\tilde{R}\uparrow,+\tilde{R}\downarrow,+\tilde{L}\uparrow,+\tilde{L}\downarrow,-\tilde{R}\uparrow,-\tilde{R}\downarrow,-\tilde{L}\uparrow,-\tilde{L}\downarrow=1,2,3,4,5,6,7,8$ and the vector $\mathbf{e}_{\alpha\tilde{r}\sigma}$ denotes a state where there is only one particle in the branch $\alpha\tilde{r}\sigma$. The notation $\Sigma_{i=1}^{\alpha\tilde{r}\sigma-1}$ means that the sum runs over all the state from 1 to $i=\alpha\tilde{r}\sigma-1$ with $\alpha\tilde{r}\sigma$ fixed by the unit vector $\mathbf{e}_{\alpha\tilde{r}\sigma}$. The phase factor is

$$K_{\alpha\tilde{r}F\sigma}(u) = \frac{1}{\sqrt{2L}} e^{i(\pi/L)\mathrm{sgn}(F)[\mathrm{sgn}(\tilde{r})N_{\alpha\tilde{r}\sigma}+\Delta_{\alpha}]u},$$

where $\Delta_{\pm}=\Delta$ for the c-DWCNTs. The field operator $\phi^{\dagger}_{\alpha\tilde{r}F\sigma}$ is given as

$$i\phi_{\alpha\tilde{r}F\sigma}(u) = \sum_{q>0}\frac{e^{-aq/2}}{\sqrt{n_q}} e^{i\,\mathrm{sgn}(\tilde{r}F)qu} b_{\alpha\,\mathrm{sgn}(\tilde{r})q\sigma}.$$

Therefore, the matrix elements of the 1D electron operator have the form[23]

$$\langle\mathbf{N},\mathbf{m}|\psi_{\alpha\tilde{r}F\sigma}(u)|\mathbf{N}',\mathbf{m}'\rangle = \delta_{\mathbf{N}+\mathbf{e}_{\alpha\tilde{r}\sigma},\mathbf{N}'}(-1)^{\sum_i^{\alpha\tilde{r}\sigma-1}N_i}\frac{e^{-(1/2)\Sigma_{q>0}e^{-aq}\Sigma_{j\delta\xi}|\lambda^{j\delta\xi F}_{\alpha\tilde{r}\sigma q}(u)|^2}}{\sqrt{1-e^{-a\pi/L}}} \times K_{\alpha\tilde{r}F\sigma}(u)\prod_{q>0}\prod_{j\delta\xi}F[\lambda^{j\delta\xi F}_{\alpha\tilde{r}\sigma q}(u),m_{j\delta\xi q},m'_{j\delta\xi q}], \quad \text{(A3)}$$

where the function F can be expressed in terms of the Laguerre polynomials L^n_m,[47]

$$F(\lambda,m,m') = \frac{m_{\min}!}{m_{\max}!}L^{m_{\max}-m_{\min}}_{m_{\min}}(|\lambda|^2)[\Theta(m'-m)\lambda^{m'-m} + \Theta(m-m')(-\lambda^*)^{m-m'}], \quad \text{(A4)}$$

with $m_{\max}=\max(m,m')$ and $m_{\min}=\min(m,m')$. $\Theta(x)$ is the Heaviside step function and the parameters λ's are given by

$$\lambda^{j\delta\xi F}_{\alpha\tilde{r}\sigma q}(u) = \frac{\Lambda^{j\delta\xi q}_{\alpha\tilde{r}\sigma}}{\sqrt{n_q}}(e^{i\,\mathrm{sgn}(\tilde{r}F)qu}S_{j\delta\xi q} - e^{-i\,\mathrm{sgn}(\tilde{r}F)qu}C_{j\delta\xi q}). \quad \text{(A5)}$$

Finally, the quantity

$$W(u) \coloneqq \frac{e^{-(1/2)\Sigma_{q>0}e^{-aq}\Sigma_{j\delta\xi}|\lambda^{j\delta\xi F}_{\alpha\tilde{r}\sigma q}(u)|^2}}{\sqrt{1-e^{-a\pi/L}}} \quad \text{(A6)}$$

is independent of $\alpha\tilde{r}\sigma$[23] and finite also in the limit $a\to 0$. It yields a nonoscillatory position dependence of the matrix elements [Eq. (A3)].

APPENDIX B: EXPRESSIONS OF THE TUNNELING RATES

In this appendix, we provide a derivation of the expressions of the tunneling rates Γ, Eqs. (53) and (54). Starting point is their definition,[23]

$$\Gamma^{(\pm)E_NE'_{N+1}}_{lk'mnk} \coloneqq \frac{1}{\hbar^2}\sum_{\alpha\sigma}\int\int d\mathbf{x}d\mathbf{y}[\Psi_{\alpha\sigma}(\mathbf{x})]^{E_NE'_{N+1}}_{k'm}[\Psi^{\dagger}_{\alpha\sigma}(\mathbf{y})]^{E'_{N+1}E_N}_{nk} \times\int_0^{\infty}dt'\mathcal{F}_{l\alpha\sigma}(\mathbf{x},\mathbf{y},\pm t')e^{\mp(i/\hbar)(E'_{N+1}-E_N)t'}, \quad \text{(B1)}$$

$$\Gamma^{(\pm)E_NE'_{N-1}}_{lk'mnk} \coloneqq \frac{1}{\hbar^2}\sum_{\alpha\sigma}\int\int d\mathbf{x}d\mathbf{y}[\Psi^{\dagger}_{\alpha\sigma}(\mathbf{x})]^{E_NE'_{N-1}}_{k'm}[\Psi_{\alpha\sigma}(\mathbf{y})]^{E'_{N-1}E_N}_{nk} \times\int_0^{\infty}dt'\mathcal{E}_{l\alpha\sigma}(\mathbf{x},\mathbf{y},\pm t')e^{\mp(i/\hbar)(E'_{N-1}-E_N)t'}, \quad \text{(B2)}$$

where $t'=t-t_1$ and $[\Psi_{\alpha\sigma}(\mathbf{x})]^{E_NE'_{N+1}}_{k'm}=\langle k'|\Psi_{\alpha\sigma}(\mathbf{x})|m\rangle$ is the matrix element of the electron operator between the states $|k\rangle$ and $|m\rangle$ with N and $N+1$ particles, respectively. The functions $\mathcal{F}_{l\alpha\sigma}$ and $\mathcal{E}_{l\alpha\sigma}$ characterizing the leads are

$$\mathcal{E}_{l\alpha\sigma}(\mathbf{x},\mathbf{y},t') = T_{l\alpha}(\mathbf{x})T^*_{l\alpha}(\mathbf{y})\langle\Phi_{l\sigma}(\mathbf{x})\Phi^{\dagger}_{l\sigma}(\mathbf{y},-t')\rangle_{\mathrm{th}} = T_{l\alpha}(\mathbf{x})T^*_{l\alpha}(\mathbf{y})\int d\varepsilon g_l(\varepsilon)[1-f(\varepsilon)] \times\sum_{\mathbf{q}|_{\varepsilon}}\phi_{l\mathbf{q}}(\mathbf{x})\phi^*_{l\mathbf{q}}(\mathbf{y})e^{-(i/\hbar)(\varepsilon-eV_l)t'}, \quad \text{(B3)}$$

$$\mathcal{F}_{l\alpha\sigma}(\mathbf{x},\mathbf{y},t') = T^*_{l\alpha}(\mathbf{x})T_{l\alpha}(\mathbf{y})\langle\Phi^{\dagger}_{l\sigma}(\mathbf{x})\Phi_{l\sigma}(\mathbf{y},-t')\rangle_{\mathrm{th}} = T^*_{l\alpha}(\mathbf{x})T_{l\alpha}(\mathbf{y})\int d\varepsilon g_l(\varepsilon)f(\varepsilon) \times\sum_{\mathbf{q}|_{\varepsilon}}\phi^*_{l\mathbf{q}}(\mathbf{x})\phi_{l\mathbf{q}}(\mathbf{y})e^{(i/\hbar)(\varepsilon-eV_l)t'}, \quad \text{(B4)}$$

where $g_l(\varepsilon)$ is the density of states in lead l, V_l is the voltage in the lead l, and $f(\varepsilon)$ is the Fermi distribution function. In the following, we shall derive the expressions for the tunneling rates $\Gamma^{(\pm)E_NE_{N+1}}_{lk'mnk}$ for an i-DWCNT QD system as an example and the expressions for the other tunneling rates can be obtained by the same method. By substituting Eqs. (B4) and (22) into Eq. (B1), we have

$$\Gamma^{(\pm)E_N E'_{N+1}}_{lk'mnk} = \frac{L}{\hbar^2}\sum_{\alpha\sigma}\sum_{\tilde{r}\tilde{r}'}\sum_{FF'} \mathrm{sgn}(FF') \int\int d\mathbf{x}d\mathbf{y}\varphi_{\alpha\,\mathrm{sgn}(F)\tilde{r}F}(\mathbf{x})\varphi^*_{\alpha\,\mathrm{sgn}(F')\tilde{r}'F'}(\mathbf{y})T^*_{l\alpha}(\mathbf{x})T_{l\alpha}(\mathbf{y})$$
$$\times \int d\varepsilon \int_0^\infty dt' e^{\pm(i/\hbar)(\varepsilon - eV_l - E'_{N+1}+E_N)t'} g_l(\varepsilon)f(\varepsilon)\sum_{\mathbf{q}|_\varepsilon}\phi^*_{l\mathbf{q}}(\mathbf{x})\phi_{l\mathbf{q}}(\mathbf{y})[\psi_{\alpha\tilde{r}\sigma F}(u_l)]^{E_N E'_{N+1}}_{k'm}[\psi^\dagger_{\alpha\tilde{r}'\sigma F'}(u_l)]^{E'_{N+1}E_N}_{nk}, \quad \text{(B5)}$$

where $u_l=0,L$ for $l=s,d$. We ignore the slow oscillations of the 1D electron operators on the scale of the extension of the tunneling region and therefore the product $[\psi_{\alpha\tilde{r}\sigma F}(u_l)]^{E_N E'_{N+1}}_{k'm}[\psi^\dagger_{\alpha\tilde{r}'\sigma F'}(u_l)]^{E'_{N+1}E_N}_{nk}$ is independent of the position. We thus obtain

$$\Gamma^{(\pm)E_N E'_{N+1}}_{lk'mnk} = \frac{L}{\hbar^2}\sum_{\alpha\sigma}\sum_{\tilde{r}\tilde{r}'}\sum_{FF'} \mathrm{sgn}(FF') \int d\varepsilon g_l(\varepsilon)f(\varepsilon)I_{l\alpha FF'\tilde{r}\tilde{r}'}(\varepsilon)\int_0^\infty dt' e^{\pm(i/\hbar)(\varepsilon - eV_l - E'_{N+1}+E_N)t'}[\psi_{\alpha\tilde{r}\sigma F}(u_l)]^{E_N E'_{N+1}}_{k'm}[\psi^\dagger_{\alpha\tilde{r}'\sigma F'}(u_l)]^{E'_{N+1}E_N}_{nk}, \quad \text{(B6)}$$

where

$$I_{l\alpha FF'\tilde{r}\tilde{r}'}(\varepsilon) = \int\int d\mathbf{x}d\mathbf{y}\varphi_{\alpha\,\mathrm{sgn}(F)\tilde{r}F}(\mathbf{x})\varphi^*_{\alpha\,\mathrm{sgn}(F')\tilde{r}'F'}(\mathbf{y})$$
$$\times T^*_{l\alpha}(\mathbf{x})T_{l\alpha}(\mathbf{y})\sum_{\mathbf{q}|_\varepsilon}\phi^*_{l\mathbf{q}}(\mathbf{x})\phi_{l\mathbf{q}}(\mathbf{y}). \quad \text{(B7)}$$

The integrals over ε and t' can be carried out by using the relation, valid for any smooth function $G(\varepsilon)$,

$$\int d\varepsilon G(\varepsilon)\int_0^\infty dt' e^{\pm(i/\hbar)(\varepsilon-E)t'} = \pi\hbar G(E) \pm i\hbar\mathcal{P}\int\frac{G(\varepsilon)}{\varepsilon - E}d\varepsilon,$$

with $\mathcal{P}$ denoting the Cauchy principal value. Let us, however, first focus on the part depending on the position in Eq. (B6), namely, on Eq. (B7). Because the Bloch waves $\varphi_{\alpha\,\mathrm{sgn}(F)\tilde{r}F}$ from Eq. (6) are localized around the carbon atoms and on the length scale of the p_z orbitals all the other quantities in Eq. (B7) are slowly varying, we can rewrite the two integrals as two sums over the positions of the carbon atoms and Eq. (B7) becomes

$$I_{l\alpha FF'\tilde{r}\tilde{r}'} = \frac{C}{N_\alpha}\sum_{\mathbf{R}p}\sum_{\mathbf{R}'p'} e^{i\mathbf{F}\cdot\mathbf{R}}e^{i\mathbf{F}'\cdot\mathbf{R}'}f_{\alpha p\,\mathrm{sgn}(F)\tilde{r}F}f^*_{\alpha p'\,\mathrm{sgn}(F')\tilde{r}'F'}$$
$$\times T^*_{l\alpha}(\mathbf{x}_{\mathbf{R},p})T_{l\alpha}(\mathbf{y}_{\mathbf{R}',p'})\sum_{\mathbf{q}|_\varepsilon}\phi^*_{l\mathbf{q}}(\mathbf{x}_{\mathbf{R},p})\phi_{l\mathbf{q}}(\mathbf{y}_{\mathbf{R}',p'}), \quad \text{(B8)}$$

where the constant C denotes the integration over the p_z orbitals. Because the leads are described by three-dimensional Fermi gases, the wave functions $\phi_{l\mathbf{q}}(\mathbf{x})$ are the plane waves,

$$\phi_{l\mathbf{q}}(\mathbf{x}) = \frac{1}{\sqrt{V_l}}e^{i\mathbf{q}\cdot\mathbf{x}},$$

with the volume of the gas V_l. The sum over the possible orientations of $\mathbf{q}$ can be performed

$$\sum_{\mathbf{q}|_\varepsilon}\phi^*_{l\mathbf{q}}(\mathbf{x})\phi_{l\mathbf{q}}(\mathbf{y}) \approx \frac{4\pi\sin(q|_\varepsilon|\mathbf{x}-\mathbf{y}|)}{q|_\varepsilon|\mathbf{x}-\mathbf{y}|},$$

which is peaked around $\mathbf{x}=\mathbf{y}$. For normal metals, e.g., gold, the Fermi wave vectors of the leads obey the relation $k_F > 1/a_0$, where a_0 is the nearest neighbor distance on a graphene lattice. For $q|_\varepsilon \approx k_F$, the above expression can then be approximated by two Kronecker δ's,

$$\sum_{\mathbf{q}|_\varepsilon}\phi^*_{\mathbf{q}}(\mathbf{x}_{\mathbf{R},p})\phi_{\mathbf{q}}(\mathbf{y}_{\mathbf{R}',p'}) \approx 4\pi\delta_{\mathbf{R}\mathbf{R}'}\delta_{pp'}.$$

Therefore, Eq. (B8) becomes

$$I_{l\alpha FF'\tilde{r}\tilde{r}'} = \frac{4\pi C}{N_\alpha}\sum_{\mathbf{R}p} e^{i(\mathbf{F}-\mathbf{F}')\cdot\mathbf{R}}f_{\alpha p\,\mathrm{sgn}(F)\tilde{r}F}f^*_{\alpha p\,\mathrm{sgn}(F')\tilde{r}'F'}$$
$$\times T^*_{l\alpha}(\mathbf{x}_{\mathbf{R},p})T_{l\alpha}(\mathbf{y}_{\mathbf{R},p}). \quad \text{(B9)}$$

Because of the fast oscillating phase $e^{i(\mathbf{F}-\mathbf{F}')\cdot\mathbf{R}}$, the quantity $I_{l\alpha FF'\tilde{r}\tilde{r}'}$ is nonzero only if $F=F'$. Moreover, we assume that both sublattices are equally coupled to the leads, such that the sum over $\mathbf{R}$ should give approximately the same result for $p=\pm$. Hence, we can separate the sum over p and obtain

$$\sum_p f_{\alpha p\,\mathrm{sgn}(F)\tilde{r}F}f^*_{\alpha p\,\mathrm{sgn}(F)\tilde{r}'F} = \delta_{\tilde{r}\tilde{r}'},$$

which can be easily verified by using the explicit expressions Eqs. (7) and (8). Equation (B9) becomes

$$I_{l\alpha FF'\tilde{r}\tilde{r}'} = \frac{4\pi C}{N_\alpha}\sum_{\mathbf{R}p}|T^*_{l\alpha}(\mathbf{x}_{\mathbf{R},p})|^2\delta_{FF'}\delta_{\tilde{r}\tilde{r}'}. \quad \text{(B10)}$$

By substituting Eq. (B10) into Eq. (B5), we find

$$\Gamma_{lk'mnk}^{(\pm)E_N E'_{N+1}} = \sum_{\alpha} \frac{4\pi CL}{N_\alpha \hbar^2} \sum_{\mathbf{R}p} |T_{l\alpha}(\mathbf{x}_{\mathbf{R},p})|^2 \int d\varepsilon g_l(\varepsilon) f(\varepsilon) \times \int_0^\infty dt' e^{\pm(i/\hbar)(\varepsilon - eV_l - E'_{N+1} + E_N)t'} \times \sum_{\tilde{r}\sigma F} [\psi_{\alpha\tilde{r}\sigma F}(u_l)]_{k'm}^{E_N E'_{N+1}} [\psi^\dagger_{\alpha\tilde{r}\sigma F}(u_l)]_{nk}^{E'_{N+1} E_N}. \tag{B11}$$

It is convenient to introduce the rate $\gamma_{l\alpha}(\varepsilon)$ describing the coupling strengths between the shell α in an i-DWCNTs and the lead l,

$$\gamma_{l\alpha}(\varepsilon) = \frac{8\pi^3 C g_l(\varepsilon) W^2(u_l)}{N_\alpha} \sum_{\mathbf{R}p} |T_{l\alpha}(\mathbf{x}_{\mathbf{R},p})|^2.$$

Hence, using Eq. (A3) for the matrix elements of the electron operators, we finally obtain the expression of the tunneling rates,

$$\Gamma_{lk'mnk}^{(\pm)E_N E'_{N+1}} = \frac{1}{4\pi^2\hbar^2} \sum_{\alpha} \int d\varepsilon \gamma_{l\alpha}(\varepsilon) f(\varepsilon) \times \int_0^\infty dt' e^{\pm(i/\hbar)(\varepsilon - eV_l - E'_{N+1} + E_N)t'} \sum_{\tilde{r}\sigma F} \delta_{\mathbf{N}+\mathbf{e}_{\alpha\tilde{r}\sigma},\mathbf{N}+1} \times \prod_{q>0} \prod_{q'>0} \prod_{j\delta\xi} \prod_{j'\delta'\xi'} F[\lambda_{\alpha\tilde{r}\sigma q}^{j\delta\xi F}(u_l), k'_{j\delta\xi q}, m_{j\delta\xi q}] \times F^*[\lambda_{\alpha\tilde{r}\sigma q}^{j'\delta'\xi' F}(u_l), n_{j'\delta'\xi' q'}, k_{j'\delta'\xi' q'}], \tag{B12}$$

where the vector $\mathbf{e}_{\alpha\tilde{r}\sigma}$ denotes a state with one particle in the branch $\alpha\tilde{r}\sigma$. The function $F(\lambda, m, m')$ is given in Eq. (A4) and the parameters $\lambda_{\alpha\tilde{r}\sigma}^{j\delta\xi F}$ are defined in Eq. (A5). The four eigenstates are

$$|k'\rangle = |\mathbf{N}, \mathbf{k}'\rangle, \quad |m\rangle = |\mathbf{N}+\mathbf{1}, \mathbf{m}\rangle,$$

$$|n\rangle = |\mathbf{N}+\mathbf{1}, \mathbf{n}\rangle, \quad |k\rangle = |\mathbf{N}, \mathbf{k}\rangle.$$

Similarly, the expression for the tunneling rates out of the dot is

$$\Gamma_{lk'mnk}^{(\pm)E_N E'_{N-1}} = \frac{1}{4\pi^2\hbar^2} \sum_{\alpha} \int d\varepsilon \gamma_{l\alpha}(\varepsilon)[1 - f(\varepsilon)] \times \int_0^\infty dt' e^{\mp(i/\hbar)(\varepsilon - eV_l + E'_{N-1} - E_N)t'} \sum_{\tilde{r}\sigma F} \delta_{\mathbf{N}-\mathbf{e}_{\alpha\tilde{r}\sigma},\mathbf{N}-1} \times \prod_{q>0} \prod_{q'>0} \prod_{j\delta\xi} \prod_{j'\delta'\xi'} F[\lambda_{\alpha\tilde{r}\sigma q}^{j\delta\xi F}(u_l), k'_{j\delta\xi q}, m_{j\delta\xi q}] \times F^*[\lambda_{\alpha\tilde{r}\sigma q}^{j'\delta'\xi' F}(u_l), n_{j'\delta'\xi' q'}, k_{j'\delta'\xi' q'}], \tag{B13}$$

with the eigenstates

$$|k'\rangle = |\mathbf{N}, \mathbf{k}'\rangle, \quad |m\rangle = |\mathbf{N}-\mathbf{1}, \mathbf{m}\rangle,$$

$$|n\rangle = |\mathbf{N}-\mathbf{1}, \mathbf{n}\rangle, \quad |k\rangle = |\mathbf{N}, \mathbf{k}\rangle.$$

From the expressions of the tunneling rate, Eqs. (53) and (54), we can see clearly that the contacts do not mix the electrons in different branches. We notice that in the absence of bosonic excitations, the rates simplify enormously to the form

$$\Gamma_{lk'mnk}^{(\pm)E_N E'_{N+1}} = \frac{1}{4\pi^2\hbar^2} \sum_{\alpha} \int d\varepsilon \gamma_{l\alpha}(\varepsilon) f(\varepsilon) \times \int_0^\infty dt' e^{\pm(i/\hbar)(\varepsilon - eV_l - E'_{N+1} + E_N)t'} \sum_{\tilde{r}\sigma F} \delta_{\mathbf{N}+\mathbf{e}_{\alpha\tilde{r}\sigma},\mathbf{N}+\mathbf{1}}, \tag{B14}$$

$$\Gamma_{lk'mnk}^{(\pm)E_N E'_{N-1}} = \frac{1}{4\pi^2\hbar^2} \sum_{\alpha} \int d\varepsilon \gamma_{l\alpha}(\varepsilon)[1 - f(\varepsilon)] \times \int_0^\infty dt' e^{\mp(i/\hbar)(\varepsilon - eV_l + E'_{N-1} - E_N)t'} \sum_{\tilde{r}\sigma F} \delta_{\mathbf{N}-\mathbf{e}_{\alpha\tilde{r}\sigma},\mathbf{N}-\mathbf{1}}. \tag{B15}$$

[1] S. Ijima, Nature (London) **354**, 56 (1991).
[2] R. Saito, G. Dresselhaus, and M. S. Dresselhaus, *Physical Properties of Carbon Nanotubes* (Imperial College Press, London, 1998).
[3] J.-C. Charlier, X. Blase, and S. Roche, Rev. Mod. Phys. **79**, 677 (2007).
[4] *Understanding Carbon Nanotubes*, Lecture Notes in Physics Vol. 677, edited by A. Loiseau, P. Launois, P. Petit, S. Roche, and J. Salvetat (Springer, Berlin, 2006).
[5] R. Egger and A. O. Gogolin, Phys. Rev. Lett. **79**, 5082 (1997).
[6] R. Egger and A. O. Gogolin, Eur. Phys. J. B **3**, 281 (1998).
[7] C. Kane, L. Balents, and M. P. A. Fisher, Phys. Rev. Lett. **79**, 5086 (1997).
[8] M. Bockrath, D. H. Cobden, J. Lu, A. G. Rinzler, R. E. Smalley, L. Balents, and P. L. McEuen, Nature (London) **397**, 598 (1999).
[9] H. Postma, T. Teepen, Z. Yao, M. Grifoni, and C. Dekker, Science **293**, 76 (2001).
[10] H. Ishii, H. Kataura, H. Shiozawa, H. Yoshioka, H. Otsubo, Y. Takayama, T. Miyahara, S. Suzuki, Y. Achiba, and M. Nakatake, Nature (London) **426**, 5404 (2003).
[11] J. Lee, S. Eggert, H. Kim, S.-J. Kahng, H. Shinohara, and Y. Kuk, Phys. Rev. Lett. **93**, 166403 (2004).
[12] N. Y. Kim, P. Recher, W. D. Oliver, Y. Yamamoto, J. Kong, and H. Dai, Phys. Rev. Lett. **99**, 036802 (2007).
[13] W. Liang, M. Bockrath, and H. Park, Phys. Rev. Lett. **88**, 126801 (2002).
[14] S. Moriyama, T. Fuse, M. Suzuki, Y. Aoyagi, and K. Ishibashi, Phys. Rev. Lett. **94**, 186806 (2005).
[15] S. Sapmaz, P. Jarillo-Herrero, J. Kong, C. Dekker, L. P. Kouwen-

hoven, and H. S. J. van der Zant, Phys. Rev. B **71**, 153402 (2005).
[16] S. Sapmaz, P. Jarillo-Herrero, L. Kouwenhoven, and H. van der Zant, Semicond. Sci. Technol. **21**, S52 (2006).
[17] *Single Electron Tunneling*, edited by H. Grabert and M. Devoret (Plenum, New York, 1991).
[18] Y. Alhassid, Rev. Mod. Phys. **72**, 895 (2000).
[19] D. H. Cobden and J. Nygård, Phys. Rev. Lett. **89**, 046803 (2002).
[20] Y. Oreg, K. Byczuk, and B. I. Halperin, Phys. Rev. Lett. **85**, 365 (2000).
[21] L. Mayrhofer and M. Grifoni, arXiv:0708.1486 (unpublished).
[22] L. Mayrhofer and M. Grifoni, Phys. Rev. B **74**, 121403(R) (2006).
[23] L. Mayrhofer and M. Grifoni, Eur. Phys. J. B **56**, 107 (2007).
[24] C. Schönenberger, A. Bachtold, C. Strunk, J.-P. Salvetat, and L. Forro, Appl. Phys. A: Mater. Sci. Process. **69**, 283 (1999).
[25] A. Bachtold, M. de Jonge, K. Grove-Rasmussen, P. L. McEuen, M. Buitelaar, and C. Schönenberger, Phys. Rev. Lett. **87**, 166801 (2001).
[26] E. Graugnard, P. J. de Pablo, B. Walsh, A. W. Ghosh, S. Datta, and R. Reifenberger, Phys. Rev. B **64**, 125407 (2001).
[27] R. Tarkiainen, M. Ahlskog, J. Penttila, L. Roschier, P. Hakonen, M. Paalanen, and E. Sonin, Phys. Rev. B **64**, 195412 (2001).
[28] M. R. Buitelaar, A. Bachtold, T. Nussbaumer, M. Iqbal, and C. Schönenberger, Phys. Rev. Lett. **88**, 156801 (2002).
[29] R. Egger, Phys. Rev. Lett. **83**, 5547 (1999).
[30] R. Egger and A. O. Gogolin, Phys. Rev. Lett. **87**, 066401 (2001).
[31] S. Wang and M. Grifoni, Phys. Rev. Lett. **95**, 266802 (2005).
[32] Y.-G. Yoon, P. Delaney, and S. G. Louie, Phys. Rev. B **66**, 073407 (2002).
[33] S. Roche, F. Triozon, A. Rubio, and D. Mayou, Phys. Rev. B **64**, 121401(R) (2001).
[34] F. Triozon, S. Roche, A. Rubio, and D. Mayou, Phys. Rev. B **69**, 121410(R) (2004).
[35] R. Saito, G. Dresselhaus, and M. S. Dresselhaus, J. Appl. Phys. **73**, 494 (1993).
[36] S. Uryu, Phys. Rev. B **69**, 075402 (2004).
[37] S. Uryu and T. Ando, Phys. Rev. B **72**, 245403 (2005).
[38] F. Haldane, J. Phys. C **14**, 2585 (1981).
[39] J. Voit, Rep. Prog. Phys. **57**, 977 (1994).
[40] J. von Delft and H. Schoeller, Ann. Phys. **7**, 225 (1998).
[41] T. Giamarchi, *Quantum Physics in One Dimension* (Oxford University Press, New York, 2004).
[42] K. A. Matveev and L. I. Glazman, Phys. Rev. Lett. **70**, 990 (1993).
[43] K. Blum, *Density Matrix Theory and Applications* (Plenum, New York, 1996).
[44] M. Thorwart, R. Egger, and M. Grifoni, Phys. Rev. B **72**, 035330 (2005).
[45] F. Bloch, Phys. Rev. **105**, 1206 (1957).
[46] A. Redfield, IBM J. Res. Dev. **1**, 19 (1957).
[47] I. S. Gradshteyn and I. Ryzhik, *Table of Integral, Series and Products* (Academic, San Diego, 2000).
[48] L. I. Glazman and K. A. Matveev, JETP Lett. **48**, 445 (1988).
[49] C. W. J. Beenakker, Phys. Rev. B **44**, 1646 (1991).